Coupling between fast and slow oscillator circuits in *Cancer borealis* is temperature compensated

Powell, D.J.*[1] dpowell@bowdoin.edu https://orcid.org/0000-0002-9210-2201

Haddad, S.A.*[2] sara.haddad@mls.uzh.ch https://orcid.org/0000-0003-0807-0823

Gorur-Shandilya, S.* srinivasgs@brandeis.edu https://orcid.org/0000-0002-7429-457X

Marder, E. marder@brandeis.edu https://orcid.org/0000-0001-9632-5448

Biology Department and Volen Center, Brandeis University, Waltham, MA 02454

Corresponding author: Eve Marder marder@brandeis.edu

*Authors contributed equally to this work

[1] Present address:
Biology Department
Bowdoin College
255 Maine St.
Brunswick, ME 04011

[2] Present address:
Department of Molecular Life Sciences
University of Zürich, Irchel
Winterthurerstrasse 190
CH-8057 Zürich, Switzerland

Key Words: pyloric rhythm, gastric mill rhythm, stomatogastric ganglion, central pattern generator, integer coupling

Abbreviated title: Stable temperature coupling of fast and slow oscillators

Contributions: project conception: SAH, DJP, EM; data collection: SAH, DJP; data analysis: SGS; Figure creation: SGS, DJP; manuscript writing and editing: DJP SAH SGS EM

Acknowledgments: We thank Dr. Michael P Nusbaum for insights relevant to the operation of the gastric mill circuit.

Research supported by: 5T32-NS007292 (SGS); R35-NS097343 (EM)

Abstract

Coupled oscillatory circuits are ubiquitous in nervous systems. Given that most biological processes are temperature sensitive, it is remarkable that the neuronal circuits of poikilothermic animals can maintain coupling across a wide range of temperatures. Within the stomatogastric ganglion (STG) of the crab, *Cancer borealis*, the fast pyloric rhythm (~1Hz) and the slow gastric mill rhythm (~0.1Hz) are precisely coordinated at ~11°C such that there is an integer number of pyloric cycles per gastric mill cycle (integer coupling). Upon increasing temperature from 7-23°C, both oscillators showed similar temperature-dependent increases in cycle frequency, and integer coupling between the circuits was conserved. Thus, although both rhythms show temperature dependent changes in rhythm frequency, the processes that couple these circuits maintain their coordination over a wide range of temperature. Such robustness to temperature changes could be part of a toolbox of processes that enables neural circuits to maintain function despite global perturbations.

Introduction

Coupled oscillators are common in nervous systems. Although oscillatory circuits may have distinct frequencies and duty cycles, coordination between them is often necessary for proper function (Nadim et al., 1998; Bartos et al., 1999; Colgin, 2011; Gordon, 2011; Jacobson et al., 2013; Rojas-Líbano et al., 2014; Harris and Gordon, 2015; Karalis et al., 2016; Tamura et al., 2017). For example, theta frequency circuits coupled to those in the gamma range are thought to drive both sensory and behavioral processing (Lisman and Buzsáki, 2008; Fujisawa and Buzsáki, 2011; Gordon, 2011; Lisman and Jensen, 2013). Memory formation may rely on the phase coupling of discrete populations of neurons with distinct frequency bands in the hippocampus (Tass et al., 1998; Lisman, 2005; Montgomery and Buzsaki, 2007; Scheffer-Teixeira and Tort, 2016; Zheng et al., 2016). Network uncoupling or improper coupling may lead to disease states and circuit malfunction (Moran and Hong, 2011; Kirihara et al., 2012; de Hemptinne et al., 2013; Bahramisharif et al., 2016; Salimpour and Anderson, 2019). The coordination of oscillatory circuits, often with distinct temporal features, is therefore key to circuit function and information processing. Because fluctuations in a circuit's environment can impact function (Fonseca and Correia, 2007; Tang et al., 2010; Haddad and Marder, 2018; Haley et al., 2018; Kushinsky et al., 2019; He et al., 2020), it is important to know how robust this coordination is to externally or internally generated perturbations.

The stomatogastric ganglion (STG) of the Jonah crab, *Cancer borealis*, contains two well-characterized, coupled, oscillatory circuits with known connectivity that generate distinct rhythms with different cycle periods (Coleman et al., 1995; Nadim et

al., 1998; Marder and Bucher, 2007). The pyloric rhythm (~1 Hz) is driven by a three-neuron bursting pacemaker kernel composed of the single Anterior Burster (AB) neuron and two Pyloric Dilator (PD) neurons (Nadim et al., 1998; Marder and Bucher, 2007). The gastric mill rhythm (~0.1 Hz) is produced by activating a half-center oscillator (reciprocal inhibition that produces alternating bursts of activity) between the Lateral Gastric (LG) motor neuron and Interneuron 1 (Int1), and it depends on a complex set of mechanisms including electrical junctions, and modulatory input (Coleman and Nusbaum, 1994; Coleman et al., 1995; Bartos and Nusbaum, 1997; Nadim et al., 1998; Bartos et al., 1999; Marder and Bucher, 2007; Stein et al., 2007). Although the pyloric and gastric mill oscillators independently produce distinct rhythms (Bartos et al., 1999), the core generator neurons (AB and LG) are integer coupled to each other and influence one another (Coleman and Nusbaum, 1994; Marder et al., 1998; Nadim et al., 1998).

In the New England Atlantic Ocean, where *C. borealis* is found, intertidal temperatures normally range from 8-24°C during the summer and 3-18°C in the winter (Stehlik et al., 1991). Because temperature affects most biological processes differently, it poses an interesting challenge for the nervous systems of poikilothermic animals that experience substantial temperature changes (Hazel and Prosser, 1974; Zečević and Levitan, 1980; Prosser and Nelson, 1981; Burrows, 1989; Foster and Robertson, 1992; Xu and Robertson, 1994; Xu and Robertson, 1996; Franz and Ronacher, 2002; Garrity et al., 2010; Marder et al., 2015). For example, the timescales of activation and inactivation of ion channels can change ~2 – 20 fold across 10°C (Q_{10}s) (Zečević et al., 1985; Klockner et al., 1990; Moran et al., 2004; Cao and Oertel, 2005; Fohlmeister et al., 2010; Tang et al., 2010; Kang et al., 2012; Robertson and Money, 2012; Yang and Zheng,

2014). Because neuron burst generation depends on many interdependent processes, if even a few key processes have Q_{10}s that are appreciably different, this could dramatically disrupt burst generation and/or alter the Q_{10} of a neuron's cycle period. Although the phase relationships between different pyloric neurons are stable between 7 and 23°C (Tang et al., 2010; Haddad and Marder, 2018), little is known about temperature compensation in the gastric mill oscillator (Städele et al., 2015) or how temperature affects coupling between the pyloric and gastric mill rhythms.

A key feature of temperature compensation in the pyloric circuit is that the pacemaker kernel of the pyloric rhythm maintains constant duty cycle across a range of temperatures (Tang et al., 2010; Rinberg et al., 2013), and this facilitates temperature compensation of neuron phase relationships in the rest of the circuit. Because the pyloric and gastric mill rhythms arise from different processes, it was not clear that the gastric mill rhythm would be phase compensated as a function of temperature, and whether the relationships between the two rhythms, such as integer coupling, would be maintained as temperature varies.

Results

Two rhythmic oscillators driven by different processes

There are two major rhythms produced by neurons in the STG. The pyloric rhythm is constitutively active, with a characteristic period of about 1 sec. The gastric mill rhythm can be evoked by stimulating projection neurons found within the commissural ganglia (CoGs), and has a characteristic period of 6-10 sec (Beenhakker et al., 2004). The modulatory commissural neuron 1 (MCN1) and commissural projection neuron 2 (CPN2) (**Fig. 1a**) evoke a gastric mill rhythm when stimulated or when they are spontaneously active (**Methods**) (Beenhakker et al., 2004).

The activity of both circuits can be monitored by extracellular recordings from the motor nerves exiting the STG. The gastric mill rhythm can be seen in the lateral gastric nerve (*lgn*), dorsal gastric nerve (*dgn*), and medial ventricular nerve (*mvn*) recordings in **Fig. 1b**. These recordings show alternating bursts of activity in the LG and Dorsal Gastric (DG) neurons, with the Gastric Mill (GM) neurons firing at the end of the LG burst. The VD (Ventricular Dilator) and IC (Inferior Cardiac) neurons, seen on the *mvn*, show an envelope of activity alternating with the LG neuron, but also fire in time with the faster pyloric rhythm seen on the lateral ventricular nerve (*lvn*) and pyloric dilator nerve (*pdn*) (**Fig. 1b**). Because the AB and PD neurons are strongly electrically coupled, the cycle period of the pyloric pacemaker can be monitored using the *pdn* (**Fig. 1b**), which contains only PD neuron action potentials. Similarly, the LG neuron indicates gastric mill rhythm cycle period (**Fig. 1b**).

Figure 1c is a connectivity diagram of neurons in the STG and shows how MCN1 and CPN2 activate the gastric mill neurons. While CPN2 drives the gastric mill circuit

via electrical synapses onto key motor neurons (LG and GM), MCN1 excites all neurons in the STG, including the pyloric pacemaker and gastric mill half-center neurons (LG and Int1) (**Fig. 1d**). Both pattern generating circuits provide feedback to these projection neurons (Norris et al., 1994; Blitz and Nusbaum, 2008, 2012; Blitz, 2017). The interactions between CPN2, MCN1, and LG shape the timing of the gastric mill rhythm along with rhythmic inhibition of Int1 by AB that allows LG to be rhythmically released from inhibition and burst (Coleman and Nusbaum, 1994; Coleman et al., 1995). The cartoon voltage traces (**Fig. 1d**) demonstrate integer coupling between the pyloric and gastric mill circuits, where rhythmic AB-inhibition of Int1 results in LG disinhibition and firing following the peak of Int1 inhibition (Nadim et al., 1998; Bartos et al., 1999) .

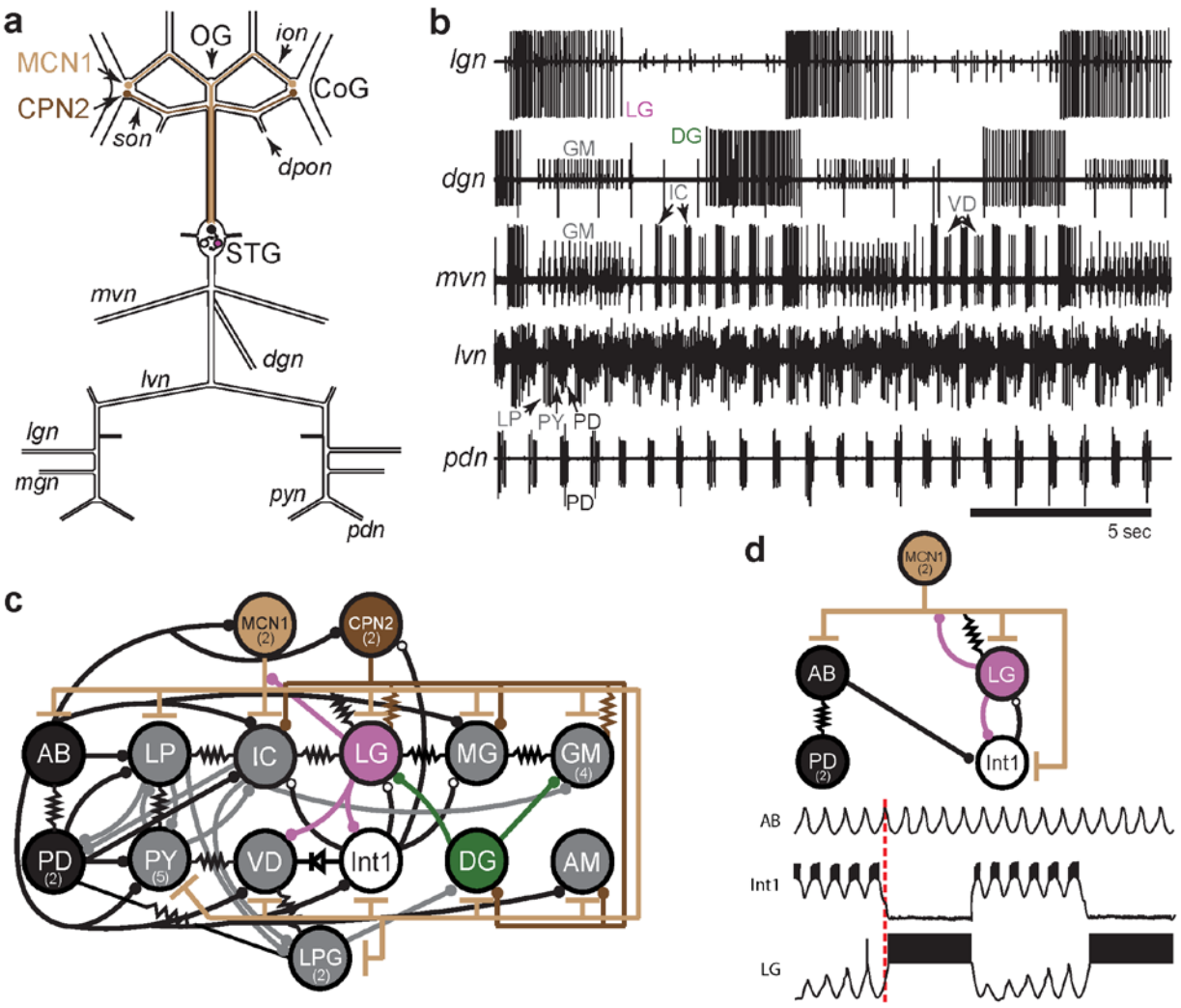

Figure 1. STG rhythmic motor patterns. (**a**) Schematic of the STNS showing the locations of salient ganglia, nerves, and projection neurons. Individual STG neurons are unambiguously identified on the basis of the motor nerves by which they project to specific stomach muscles. (**b**) Extracellular nerve recordings of both the gastric mill (*lgn*, *dgn*, *mvn*) and pyloric (*lvn*, *pdn*) rhythms. The gastric mill rhythm is seen as the alternating bursts of activity in the LG and DG neurons. The GM neurons are active late in the LG neuron burst. The IC and VD neurons are active in alternation with LG, but also show activity in time with the pyloric rhythm (*lvn)*, with the PD neurons shown on the *pdn*. (**c**) Wiring diagram of the gastric mill, pyloric, and gastropyloric neurons and the input they receive from MCN1 (tan) and CPN2 (brown) (Marder and Bucher, 2007; Blitz, 2017). LG (pink) and DG (green) are both gastric mill neurons and AB-PD (black) are pyloric neurons. Colors used for these neurons are consistent in all figures. The resistor symbols denote electrical synapses, diode symbol denotes a rectifying junction, chemical inhibitory synapses are shown as filled circles, and the T bars indicate chemical excitatory/modulatory synapses from MCN1. Neuron copy number is in parenthesis. (**d**) (Top) Simplified wiring diagram of MCN1 excitation of both pattern generating circuits and AB inhibition of Int1 (white) (Coleman and Nusbaum, 1994;

Bartos and Nusbaum, 1997). (Bottom) Cartoon voltage traces of AB, Int1, and LG as they would appear during a gastric mill rhythm showing the relative burst timing between these neurons. As a consequence of a slow excitation from MCN1 to LG, the envelope of peak disinhibition of LG (from Int1) increases slowly over several cycles, eventually resulting in LG crossing threshold and bursting in time with the AB neuron. Note the slight delays between the peak of AB depolarization, the trough of Int1 inhibition from AB, and the subsequent burst of LG as marked by the dashed line.

Spontaneous gastric mill rhythms span a physiological range of temperatures

While the circuit controlling the pyloric rhythm is temperature robust from 7°C – 25°C (Tang et al., 2010; Tang et al., 2012; Rinberg et al., 2013; Soofi et al., 2014; Haddad and Marder, 2018), it remains unclear if the gastric mill circuit could also operate across this same range (Städele et al., 2015). We inspected a dataset of extracellular recordings of *dgn* and *lgn* during temperature ramps (Haddad and Marder, 2018) and found spontaneous gastric mill activity at temperatures between 11°C and 30°C.

Figure 2a shows bursts of LG (*lgn*) and DG (*dgn*) neurons from a single preparation showing spontaneous gastric mill activity at these temperatures. While these recordings show relatively regular gastric mill rhythms at lower temperatures, they were less regular at higher temperatures. **Figure 2b** shows example raster plots of the LG neuron for two preparations with spontaneous gastric mill rhythms. Color indicates the temperature at which that rhythm was observed and can be seen in the raster plots from two preparations across a range of temperature. Preparation 1 intermittently displayed characteristic gastric mill rhythms at both high and low temperatures, but was much more irregular in the middle of the temperature range, whereas Preparation 2 was considerably less robust at high temperatures.

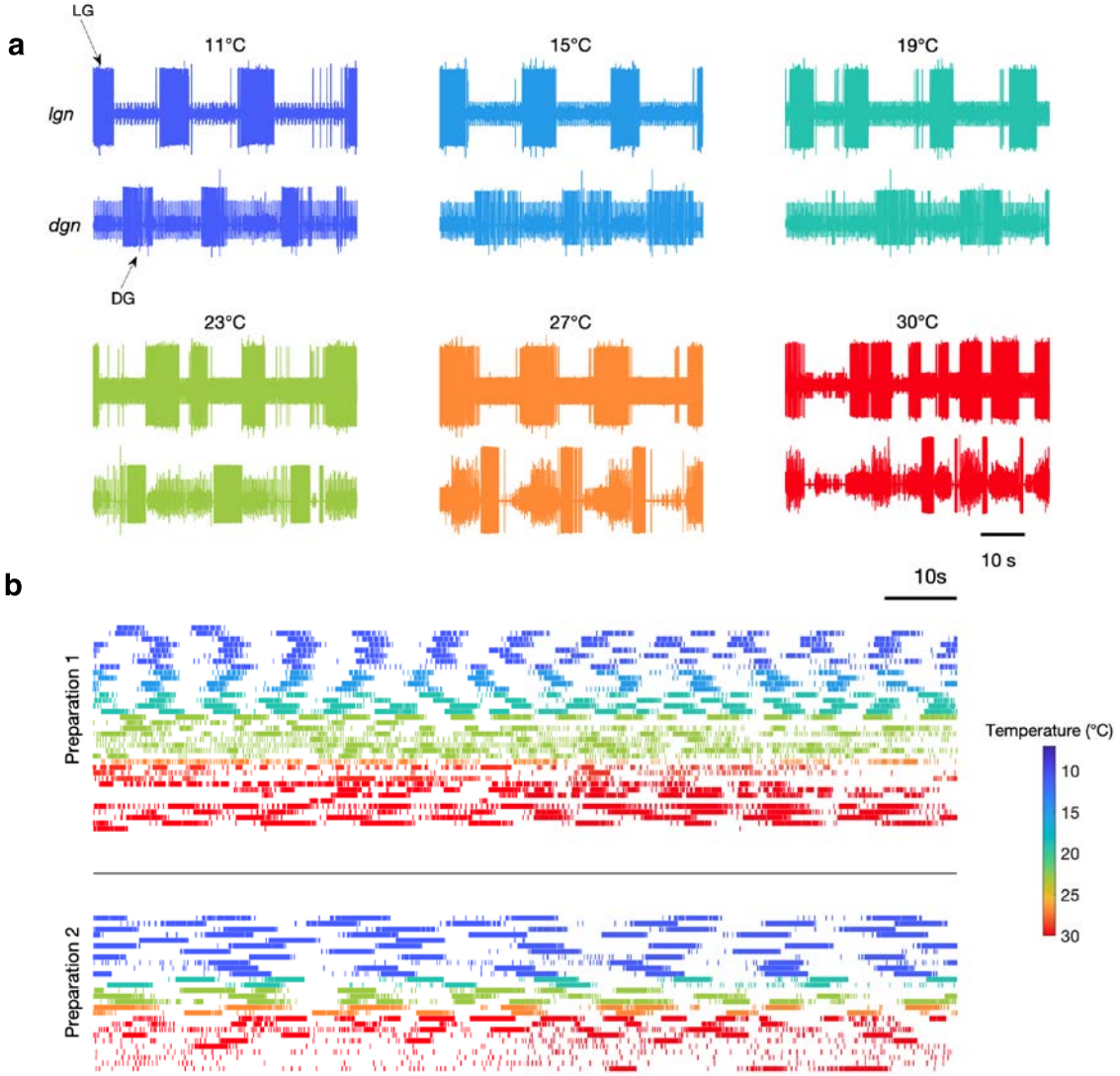

Figure 2. Spontaneous gastric mill rhythms over physiological temperature range. (**a**) Extracellular recordings from the *lgn* and *dgn* at the temperatures indicated using the color code. (**b**) Spike rasters of LG from two preparations at the indicated colors to show the activity of these preparations over extended periods of time at the indicated temperatures. Traces in (**a**) and rasters in Preparation 2 in (**b**) are from the same animal. Rasters with the same color are continuous recordings at the same temperature, and time wraps around the end of each raster and continues on the next line.

Although **Figure 2** only shows two examples of spontaneous gastric mill rhythm, there were a total of 9 preparations in which spontaneous rhythms were observed at a variety of different temperatures (**Fig. 2–figure supplement 1**). Together, these data

indicate that activating at least some combination of endogenous inputs to the gastric mill circuit can generate rhythmic activity across a wide temperature range. Nonetheless, because the cycle period of the gastric mill was often irregular in these spontaneous rhythms, we were not able to assess whether the pyloric and gastric mill circuits remained coupled. Consequently, we chose to reliably activate gastric rhythms by stimulating a known sensory pathway (**Methods**), to get a more reproducible gastric mill rhythm, of known mechanism, across temperature and across preparations.

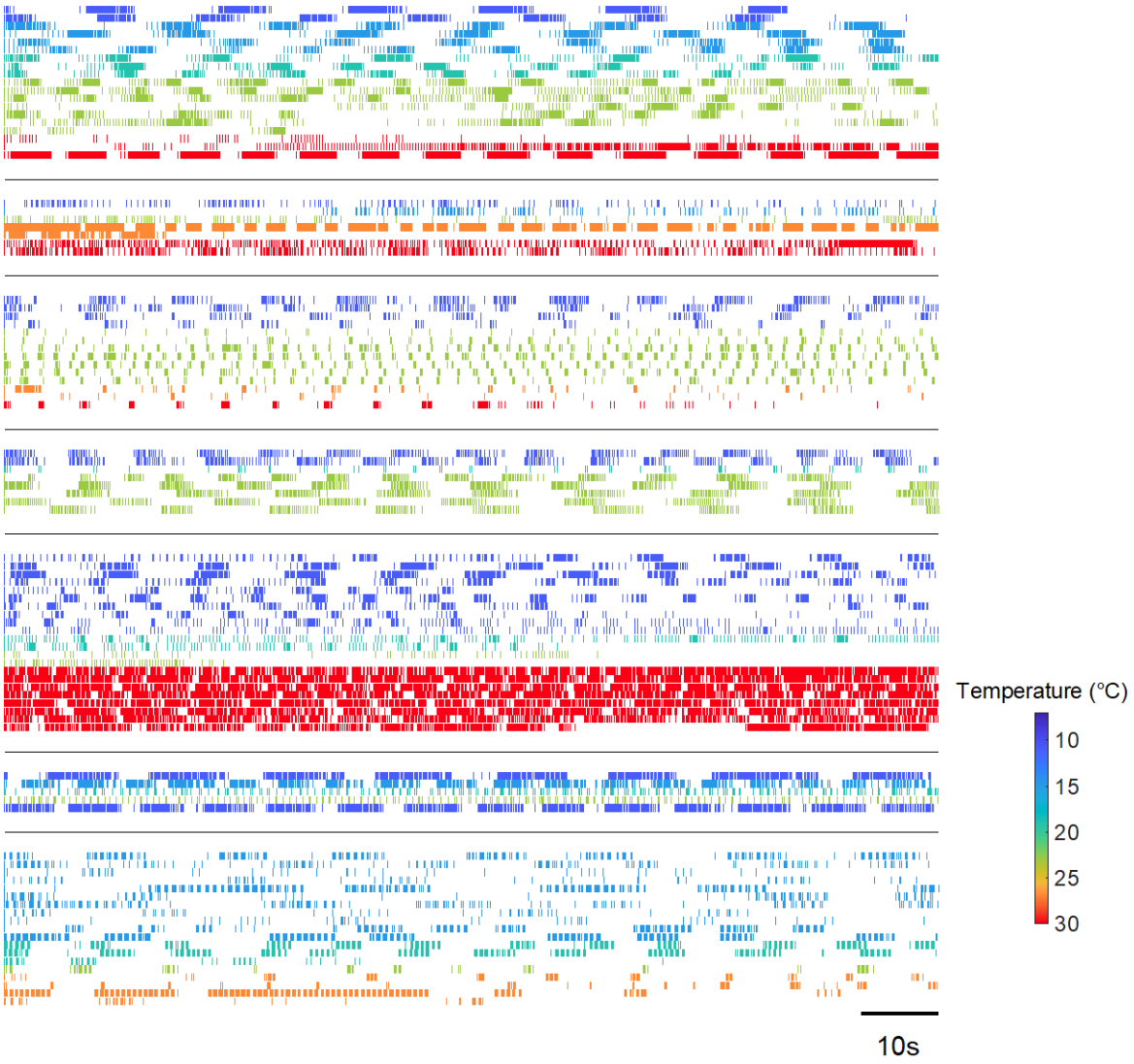

Figure 2–figure supplement 1. Spontaneous gastric activity in seven additional preparations. Each panel shows rasters of the LG neuron from a single preparation at temperatures from 11-30°C. Figure shows seven different preparations separated by black lines. LG was spontaneously active at temperatures as high as 30°C. Color of each row of raster indicates temperatures.

Gastric mill rhythms speed up with increased temperature

We were able to evoke gastric rhythms across the same temperature range at which the pyloric circuit is robust (Tang et al., 2010). **Figure 3** shows example

recordings of evoked gastric rhythms at 7°C (**Fig. 3a**) and 23°C (**Fig. 3b**). Raster plots from this preparation for the entire temperature range are shown in **Figure 3c**. Similar to the pyloric circuit, the gastric mill rhythm cycle period decreased with increased temperature from 7°C to 23°C. Although we observed that some of the neuron phase relationships (relative timing of the neurons in each cycle) were altered at 23°C (e.g. between DG and LG in **Figure 3b**), at high temperatures, the gastric mill rhythm generator still produced regular rhythmic activity following stimulation. We were able to evoke gastric rhythms across a temperature range of 7–21°C in 9/10 preparations.

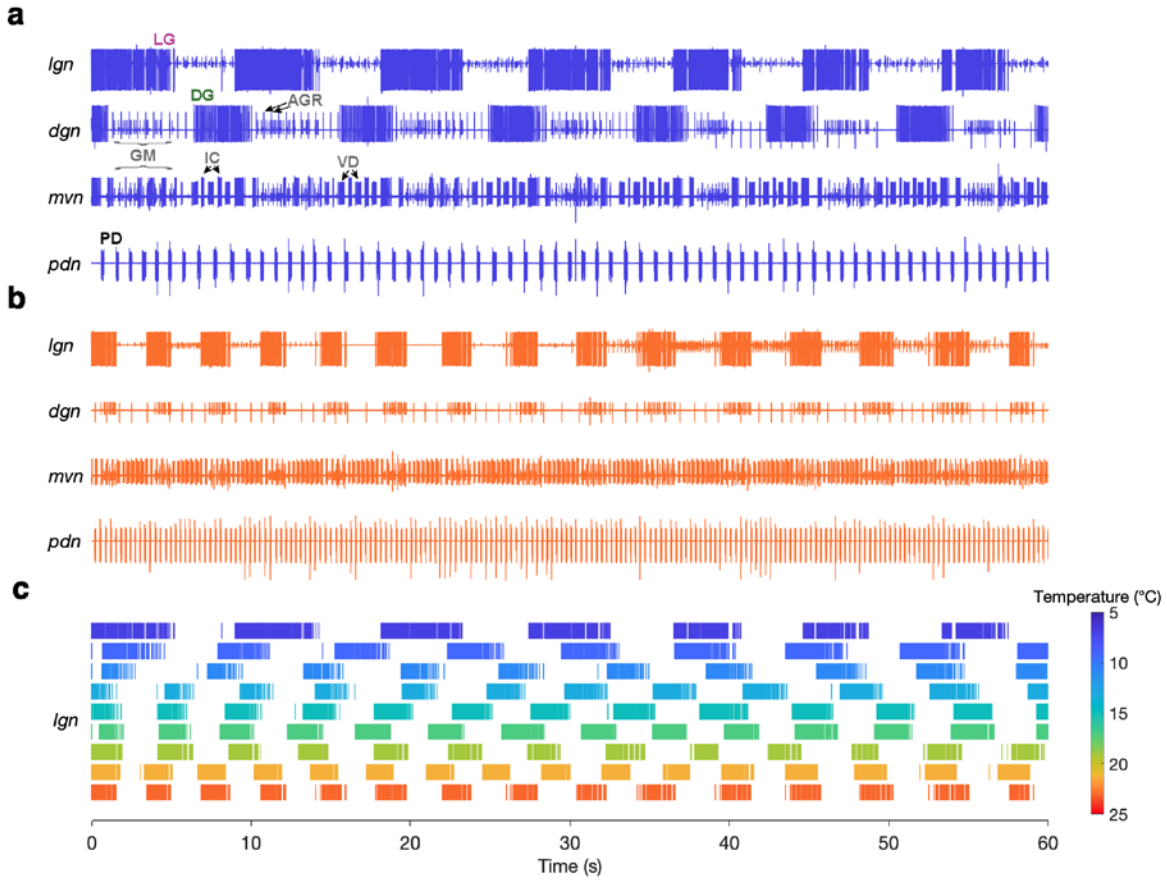

Figure 3. Gastric mill rhythms can be evoked by stimulation over physiological temperature range. (**a**) Extracellular recordings from a preparation at 7°C (blue) and (**b**) 23°C (orange). Neuron action potentials described by their relative amplitudes on each nerve: *lgn*: LG (large bursting unit); *dgn*: DG (large, bursting unit; out of phase with LG: only on 7°C trace, has ceased bursting at 23°C), AGR (tonic), GM (small bursting unit; in-phase with LG); *mvn*: IC (large bursting unit), VD (medium bursting unit, antiphase with LG, alternates with IC), GM (small bursting unit; in-phase with LG); *pdn*: PD. (**c**) Spike rasters showing the activity of the LG neuron over the entire temperature range. The first row corresponds to (**a**) and the last row corresponds to (**b**).

In some preparations (4/10), spontaneous gastric mill rhythms were observed prior to evoking a rhythm. **Figure 3–figure supplement 1a** shows example recordings of both a spontaneous (black) and evoked (blue) gastric mill rhythm from the

same preparation (11°C). Three of the four preparations that had spontaneous and evoked rhythms shared similarities in LG spike and burst timing (**Fig. 3–figure supplement 1b**) and rhythm cycle period (mean ± SD) (**Fig. 3–figure supplement 1c**). Because there are ten known processes of gastric mill rhythm generation and all but two are distinct from one another (Heinzel et al., 1993; Coleman and Nusbaum, 1994; Norris et al., 1994, 1996; Weimann et al., 1997; Blitz et al., 1999; Christie et al., 2004; Saideman et al., 2007a; Saideman et al., 2007b; White and Nusbaum, 2011; Dickinson et al., 2015; Blitz et al., 2019), similarities between spontaneous and evoked gastric mill rhythms within a preparation suggested that these rhythms are driven by similar processes.

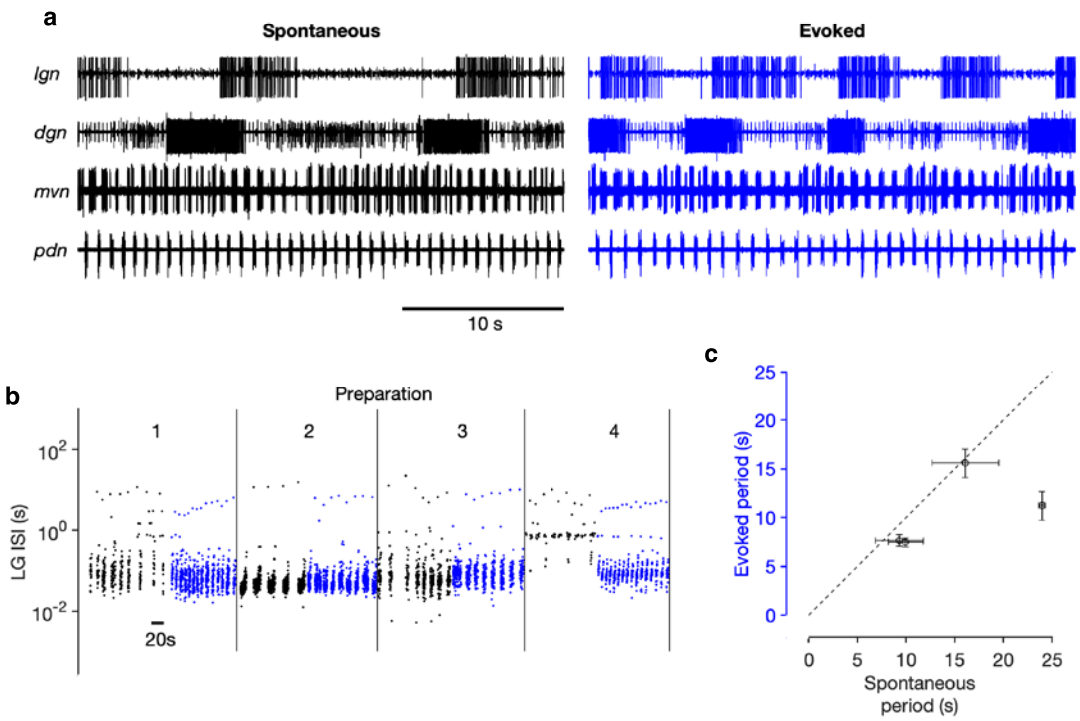

Figure 3–figure supplement 1. Comparison of spontaneous and evoked gastric mill rhythms within the same preparation. In 4/10 preparations, spontaneous gastric mill rhythms were observed at 11°C. (**a**) Extracellular traces showing activity on *lgn*, *dgn*, *mvn* and *pdn* nerves during spontaneous gastric mill activity (black) and after stimulation (blue). (**b**) Inter-spike intervals (ISIs) of LG neuron in the four preparations that showed spontaneous gastric mill activity. Black dots indicate ISIs from spontaneous activity and blue dots from evoked activity. (**c**) Comparison of burst period of LG during spontaneous and evoked bursting. Raw traces in (**a**) correspond to Preparation 1 in (**b**).

Gastric mill and pyloric cycle periods are similarly temperature sensitive

The pyloric cycle period decreases ~2-fold with a 10°C increase in temperature (Tang et al., 2010). If the pyloric and gastric mill circuits are to be coordinated across temperature, we hypothesized that the gastric mill period might also show a similar temperature dependence. We measured the burst periods of PD neurons (**Fig 4, black**) and LG neurons (**Fig 4, magenta**) in all 10 preparations in which the gastric mill

rhythm was evoked by stimulation over a temperature range from 7–21°C. **Fig 4a** shows that, in a single preparation, both LG and PD burst periods decrease with increasing temperature, despite significant variability in the LG burst period, due to a slowing down (**Figure 4 – figure supplement 1**) of the gastric mill rhythm with time since stimulation (Beenhakker et al., 2004; Stein et al., 2007).

A coordinated decrease in both gastric mill and pyloric cycle periods was observed in all ten preparations (**Fig. 4b**). We quantified the extent to which the cycle period increased with temperature using the Q_{10} (**Methods**). **Figure 4c** shows that most preparations (8 of 10) exhibited a cycle period Q_{10} of ~2 for both the pyloric and gastric mill rhythms. Estimated Q_{10}s were not significantly different for LG and PD burst periods (paired t-test, $p = 0.235, N = 10, t = 1.27$), suggesting that the periods of both circuits were not differently influenced by increased temperature.

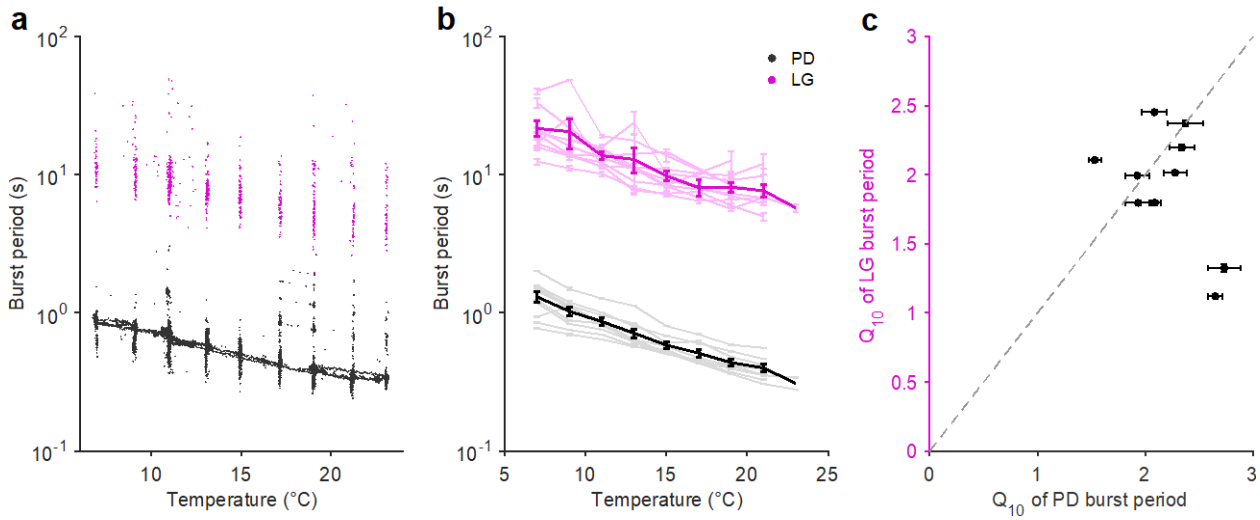

Figure 4. Pyloric and Gastric mill periods are similarly temperature sensitive. (**a**) Burst period of PD (black) and LG (magenta) in a single preparation as a function of temperature. Each dot corresponds to a single burst. (**b**) Burst period of PD and LG for ten preparations. Each line is a single preparation. Mean of all preparations shown in thick lines. (**c**) The apparent Q_{10} of the burst frequency of each preparation for the PD and LG neurons, representing the pyloric and gastric mill rhythms. The apparent Q_{10}s of the two rhythms are not significantly different (paired *t*-test, $p = 0.235, N = 10, t = 1.27$)

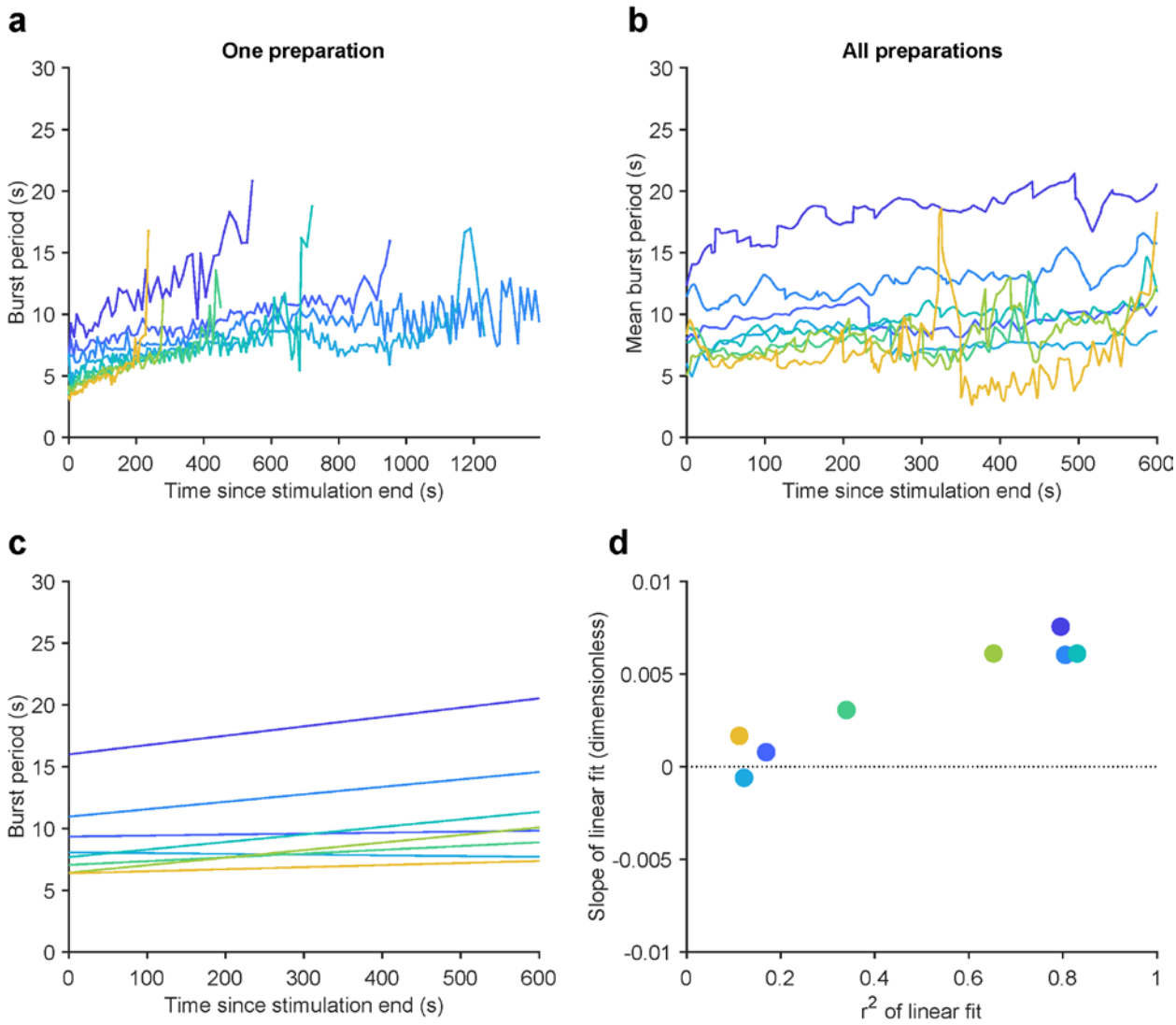

Figure 4 – figure supplement 1. Gastric mill rhythms slow down with time after stimulation. (**a**) Instantaneous LG burst period plotted against time for a single preparation. Each line shows LG burst period for each gastric mill rhythm. Lines are of varying length as gastric mill rhythm duration was different each time it is evoked (**Methods**). Colors indicate temperature (7 – 21°C). (**b**) Mean LG burst period for the first 600 seconds post-stimulation for all 10 preparations. (**c**) Linear fits for average LG burst period across all preparations at each temperature. (**d**) Slopes of the linear fits in (**c**) plotted vs. r^2 of each fit line.

Gastric mill rhythms can be evoked when the pyloric pacemaker is suppressed

At 11°C the gastric mill half-center is capable of producing rhythmic activity even if the pyloric rhythm is turned off by hyperpolarization of the pacemakers (Bartos et al., 1999). Therefore we hypothesized that the gastric mill oscillator might be independently temperature robust in the absence of pyloric input. To test this, we evoked gastric mill rhythms at 11°C, 15°C, 19°C, and 21°C with the pyloric pacemaker both active and inactive (**Methods**).

Figure 4 – figure supplement 2a and b show example recordings from a single preparation in which, at each temperature, we evoked a "control" rhythm (AB/PD active) followed by an evoked rhythm with both PD neurons hyperpolarized (AB/PD inactive). **Figure 4 – figure supplement 2c** shows that the gastric mill rhythm cycle period steadily decreased with increased temperature regardless of pyloric pacemaker activity. **Figure 4 – figure supplement 2d** shows that in all 9 preparations, the gastric mill rhythm was activated at 11°C and 15°C, whereas at 19°C and 21°C only a subset of preparations produced gastric mill rhythms at these elevated temperatures.

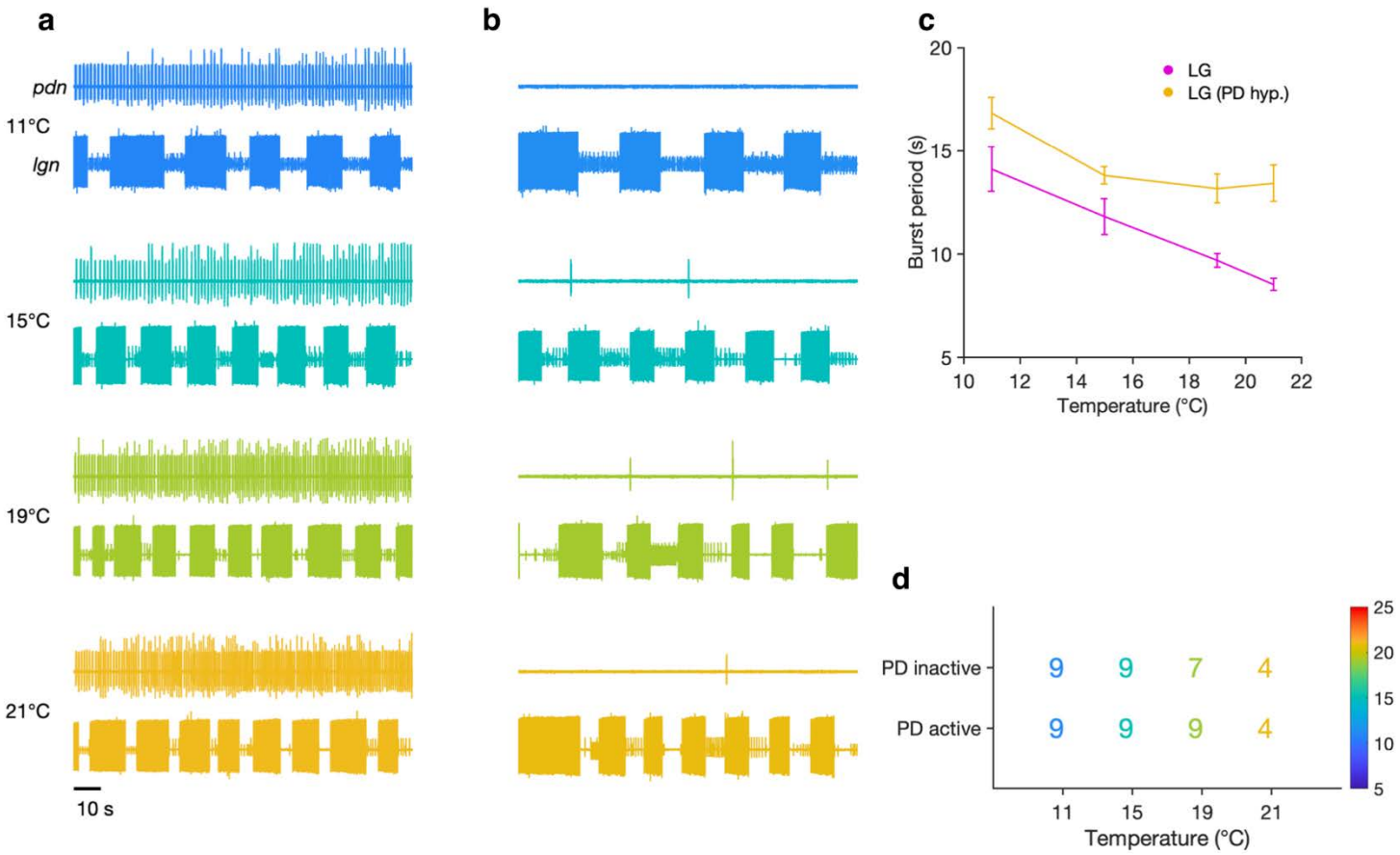

Figure 4 – figure supplement 2. Evoked gastric mill rhythms persist when the pyloric pacemaker is suppressed. Extracellular recordings of the *lgn* and *pdn* at 11°C, 15°C, 19°C, and 21°C with the pyloric pacemaker kernel active (**a**) and inactive (**b**) in a single preparation. (**c**) Burst period of LG with the pacemaker active (magenta) and inactive (yellow) at each temperature step for the preparation shown in (**a**) and (**b**) (Mean ± SEM). (**d**) Number of preparations (out of 9 total) in which a gastric mill rhythm could be evoked with the pacemaker kernel active (bottom row) and with AB/PD hyperpolarized (top row) for each temperature.

Integer coupling is maintained across a physiological temperature range

Integer coupling between two interacting oscillators with different periods refers to the phenomenon in which the slower rhythm (gastric mill) tends to have a period that is an integer multiple of the period of the faster cycle (pyloric) (Nadim et al., 1998). Integer coupling exists between the pyloric and gastric mill oscillators at 11°C (Bartos et

al., 1999; Hamood and Marder, 2015). It remains an open question if this form of precise coordination is preserved across temperature, because both oscillators change their cycle periods with temperature.

Extracellular recordings of *lgn* and *pdn* at 7°C and 23°C from the same preparation are shown in **Fig. 5a**. PD bursts tended to terminate shortly before the initiation of LG bursting at both temperatures (**Fig. 5a**, dotted vertical lines indicate start of LG bursting). The ratio of LG to PD periods was close to an integer at both temperatures (~10 at 7°C and ~11 at 23°C).

To visualize integer coupling between the PD and LG across the entire dataset, we plotted the LG burst period as a function of the mean PD burst period during that LG burst (**Fig. 5b**). Data tended to lie along lines with integer slope (gray lines), suggesting integer coupling between LG and PD across temperature. DG burst periods, which were similar to LG burst periods, did not tend to lie on lines with integer slope (**Fig. 5c**). To quantify the degree of integer coupling, we computed the cumulative distribution of significands (value after the decimal point) of the ratios of gastric mill to pyloric periods (**Fig. 5d**, **Methods**). Perfect integer coupling would lead to a cumulative distribution indicated by the dotted line, while randomly chosen significands would lie along the diagonal. Cumulative distributions for LG were skewed towards perfect integer coupling, while distributions for DG were closer to the randomly distributed significands, suggesting that integer coupling was observed in LG but not DG.

To quantify how the degree of integer coupling varies across temperature, we measured the area between the cumulative distributions and the diagonal in **Fig. 5d**. Perfect integer coupling would yield an area of 0.25. Areas for LG/PD significands were

larger than areas for DG/PD significands at every temperature (**Fig. 5e**), suggesting greater integer coupling. Areas for DG/PD significands overlapped with areas computed after shuffling gastric mill neuron (both LG and DG) and PD neuron cycle periods (gray lines, **Fig. 5e**). To determine if measured integer coupling was significantly different from chance, we used a two-sample Kolmogorov-Smirnoff test (**Methods**). LG and PD were significantly integer coupled, at temperatures from 7°C–21°C ($p < 10^{-5}, D > .24$), while DG and PD were not significantly coupled at any temperature ($p > .02, D < .16$). AB dictates the phase at which LG turns on because LG onset is timed with the peak of Int1 inhibition (Nadim et al., 1998). Because all previous studies of integer coupling were at ~11°C, it was not known if the process underlying integer coupling would shift with temperature increase. To visualize the effect of temperature on the ratio of PD to LG cycle period, we plotted the ratio of LG cycle period and PD cycle period as a function of temperature (**Fig. 5f**). At low temperatures, when integer coupling was particularly strong (as seen from the horizontal banding), these ratios were distributed over a wide range from 5-25. Ratios of LG to PD cycle period were spread across a similar range across temperature, even at higher temperatures when integer coupling was less pronounced ($p = 0.88$, $n = 3799$ PD cycles pooled across all preparations, Spearman test), suggesting that the mechanism of integer coupling was independent of the number of PD cycles to LG cycle period.

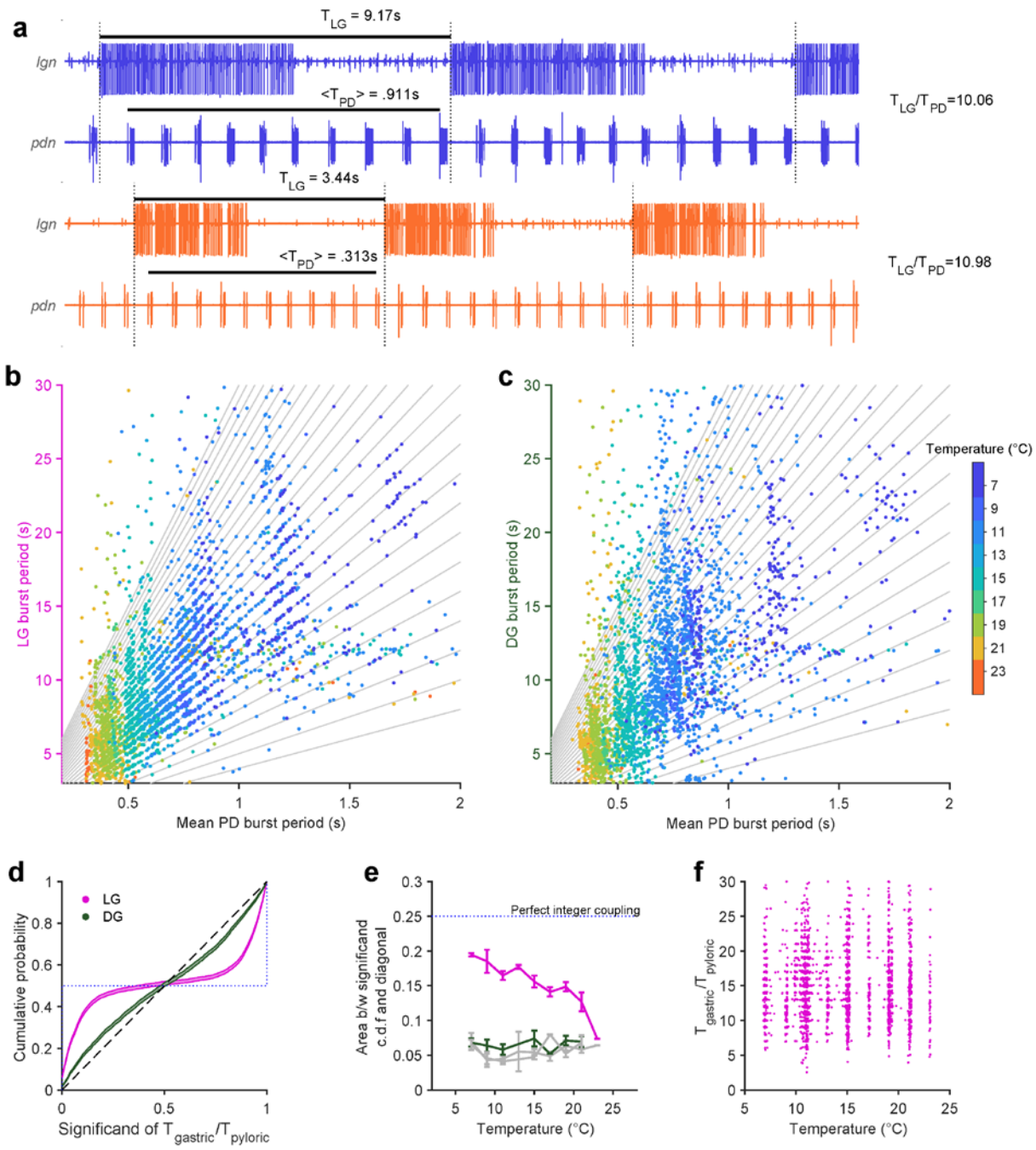

Figure 5. Integer coupling is maintained over physiological range. (**a**) Extracellular recordings of *pdn* show bursting of LG and PD at 7°C (blue) and 23°C (orange). Black bars indicate burst period of LG and mean burst period of PD. LG (**b**) and DG (**c**) burst period as a function of mean PD period. In (**b-c**), gray lines have integer slopes, and are not fits. (**d**) Cumulative probability distributions (c.d.f.s) of significand of ratio of gastric to pyloric period for LG (magenta) and DG (green) for all temperatures. Shading indicates confidence estimates from bootstrapping the data. Dashed diagonal line indicates a uniform distribution, and the dotted line indicates

perfect integer coupling. (**e**) Area between significand c.d.f.s and diagonal (a measure of how integer coupled the circuits are) as a function of temperature for all preparations. Gray lines are computed from shuffled data. LG and PD were significantly integer coupled between 7°C–21°C ($p < 10^{-6}$ two-sample Kolmogorov-Smirnoff test), while DG and PD did not exhibit integer coupling. (**f**) Ratio of gastric to pyloric periods as a function of temperature. Apparent banding along the temperature axis is a consequence of the experimental protocol, where discrete temperature steps were used (Methods). Ratios of LG to PD cycle period were similar across temperature ($p = 0.88$, Spearman test).

LG preserves phase locking to PD across physiological temperatures

How do LG and PD maintain integer coupling in their burst periods across this temperature range? One possibility is via temperature-invariant phase locking between LG and PD. If LG bursts start at a particular phase in the PD cycle, then the burst periods of LG and PD must be integer coupled (Nadim et al., 1998). We therefore set out to study the fine structure of the phase coupling between LG and PD across temperature.

To visualize the phase coupling between LG and PD, we plotted PD spikes aligned to LG burst starts (**Fig. 6a**) normalizing time by the mean PD burst period in each row. Doing this aligns all PD spikes, suggesting that LG burst starts were an excellent predictor of PD phase. To quantify this effect across all preparations, we computed probabilities of LG burst starts across the temperature range tested. LG burst start probabilities were sharply peaked (**Fig. 6b**), and were significantly different from a uniform distribution (**Fig. 6b**, dashed line, ($p < 4 \times 10^{-4}, 7.5 < z <$ 45, Rayleigh test for non − uniformity, **see Methods** for details). From 7-21°C, LG bursts started at a phase of ~0.5 in the PD cycle (**Fig. 6b, inset**), and this phase offset did not significantly trend across this temperature range ($p = 0.46$, $\rho = -.31$, Spearman test).

LG burst initiation being phase locked to PD suggests that faster dynamics in LG, such as spiking, could also be affected by PD. Modulation of LG spiking by AB/PD has been reported via feedback from AB to MCN1 and CPN2 (Blitz and Nusbaum, 2008) and possibly Int1 feedback to CPN2 (Blitz, 2017). We measured the spike probability of LG conditional on PD phase across this temperature range, and found a pronounced decrease in the probability of spiking in LG at higher temperatures (**Fig. 6c**). This decrease in LG spike probability occurred close to PD burst termination (**Fig. 6c**, horizontal bars).

Although DG bursts on the same timescale as LG, it is not directly coupled to the pyloric oscillator (**Fig. 1**) and does not show any signature of phase coupling with PD. DG bursts starts do not align with PD spikes (**Fig. 6d**), DG burst starts are not sharply peaked in PD phase, and they are not significantly different from a uniform distribution for all preparations at all temperatures (**Fig. 6e**, $p \in [.001, .85], .15 < z < 13$, Rayleigh test). DG spike probability also does not show a noticeable decrease close to the end of PD bursting (**Fig. 6f,** cf. **Fig. 6c**).

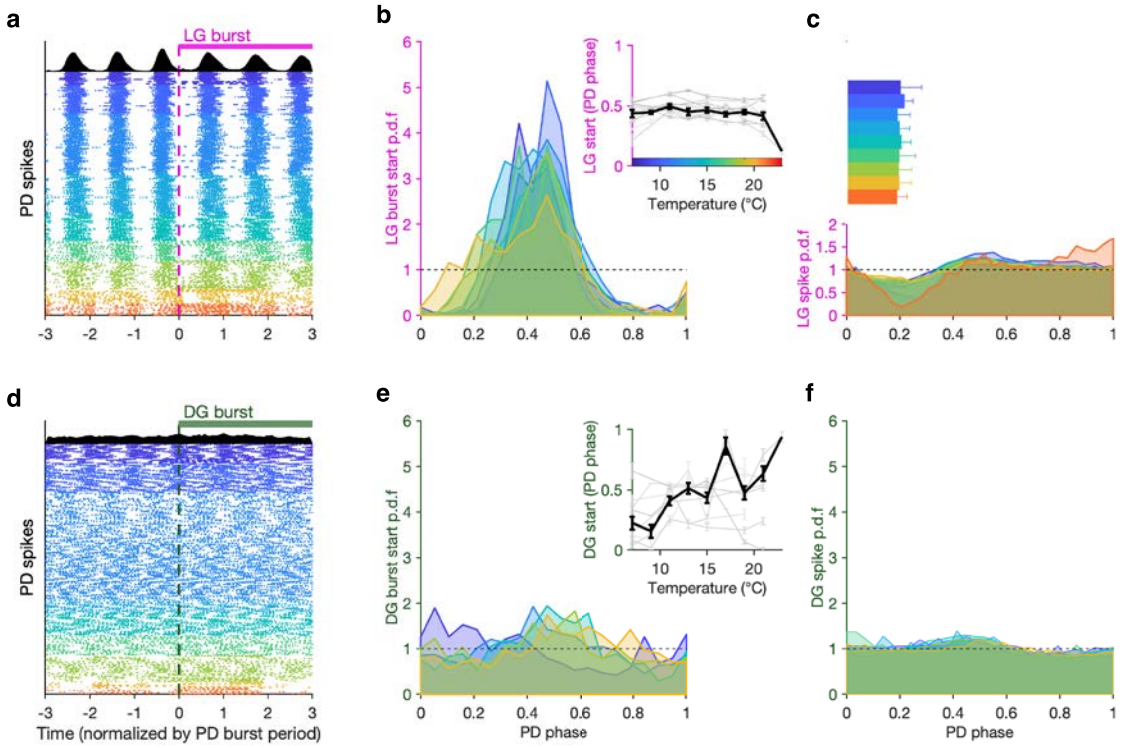

Figure 6. LG, but not DG, bursts and spikes are phase locked to PD across temperature. (**a**) PD spike rasters aligned to LG burst starts (dashed line at 0) in a single preparation. Each row corresponds to a LG burst start, and time is normalized by PD burst period. Black histograms at the top show spike probability over all rasters. (**b**) LG burst start probability as a function of PD phase. Inset shows mean LG burst start phase a function of temperature (gray lines: individual preparations, black line: mean across all preparations). LG burst start probabilities were significantly different from a uniform distribution ($p < 4 \times 10^{-4}, 7.5 < z < 45$, Rayleigh test for non-uniformity). Phase offset between LG and PD was similar from 7 to 21°C (inset, $p = 0.46$, Spearman test). (**c**) LG spike probability as a function of PD phase at various temperatures. Bars indicate PD spiking. (**d-f**) Similar to (**a-c**), but for DG. DG burst starts are not always significantly non-uniformly distributed, and the effect size is much smaller ($p \in [.001, .85], .15 < z < 13$, Rayleigh test). Rasters in (**a,d**) are from the same preparation.

Discussion

Temperature sensitive circuits maintain coordinated activity

Coupling between rhythmic circuits is common in nervous systems and is often functionally important, although the strength and the extent of inter-circuit coupling is varied (Nadim et al., 1998; Bartos et al., 1999; Colgin, 2011; Gordon, 2011; Jacobson et al., 2013; Rojas-Líbano et al., 2014; Harris and Gordon, 2015; Karalis et al., 2016; Tamura et al., 2017). Temperature is a global perturbation that influences the properties of all ion channels and synapses in neuronal circuits (Zečević et al., 1985; Janssen, 1992; Xu and Robertson, 1996; Garrity et al., 2010; Tang et al., 2010; Kang et al., 2012; Robertson and Money, 2012; Marder et al., 2015). Because each cellular and molecular process is likely to have a different temperature dependence, or Q_{10}, maintaining the function of complex physiological processes as temperature is changed is non-trivial (Du et al., 2010; Caplan et al., 2014; Roemschied et al., 2014; O'Leary and Marder, 2016; Schleimer and Schreiber, 2016). Most often, changes in temperature affect neuronal and circuit behavior (Zečević and Levitan, 1980; Prosser and Nelson, 1981; Long and Fee, 2008; Ramot et al., 2008; Garrity et al., 2010; Robertson and Money, 2012). It then becomes critical to know whether the coupling between circuits is also altered (Stiebler and Narins, 1990), or whether the relative coordination between rhythmic behaviors can be maintained as temperature changes.

Here we show that two oscillator circuits can maintain coordinated output across a range of physiologically relevant temperatures. The cardiac ganglion, another circuit in the crab which governs heartbeat, is also temperature sensitive across a range of physiological temperature, again with a Q_{10} of ~2 (Kushinsky et al., 2019). In the pyloric,

gastric mill, and cardiac circuits, rhythmicity is maintained up to a critical temperature, and this critical temperature approximates the upper range of native ambient temperatures (Tang et al., 2010; Städele et al., 2015; Kushinsky et al., 2019).

Coupling of the gastric mill and pyloric circuits is likely to be important for the crab. In the intact animal, muscle movements of the gastric mill enable ingested food to be chewed and subsequently filtered and pumped into the hindgut by the pylorus (Marder and Bucher, 2007). Coupling between these circuits coordinates the timing of chewing and filtering enabling proper flow of food through the mid-gut (Meyrand et al., 1994; Diehl et al., 2013). Furthermore, a subset of STG neurons participates in both rhythms, and therefore coupling between the pyloric and gastric mill circuits enables neurons with dual functions to maintain their appropriate participation in both rhythms (Weimann et al., 1991; Weimann and Marder, 1994; Gutierrez et al., 2013; Blitz et al., 2019).

Oscillator circuits with different periods are similarly temperature robust

Although the gastric mill and pyloric rhythms are similarly temperature sensitive, they have an approximately 10-fold difference in cycle period. The pyloric rhythm is temperature robust because the AB neuron maintains a relatively constant duty cycle across this range (Tang et al., 2010; Rinberg et al., 2013). Temperature robustness in the gastric mill rhythm arises from a different set of interdependent processes including projection neuron input, coordination of the half-center oscillator neurons LG and Int1, and feedback from LG to MCN1. The similarity between the apparent cycle period Q_{10}s of the pyloric and gastric mill rhythms was unexpected as there are so many different

physiological processes generating the two rhythms. Moreover, a lock step variance in cycle period is not necessary in order to maintain coupling as the relative number of pyloric cycles between each gastric cycle can vary widely while circuits remain coupled (Nadim et al., 1998; Bartos et al., 1999). Because the salient drivers of LG firing are sufficient projection neuron excitation and disinhibition from Int1 (Bartos et al., 1999; DeLong et al., 2009), the total number of pyloric cycles per gastric mill cycle can vary greatly.

Spontaneous gastric mill rhythms were non-stationary and driven by unknown processes

As spontaneous gastric mill activity was often irregular, it was difficult to examine coupling between the two rhythm generating circuits. The observed irregularity could be due to weak activation of one or more descending pathways and is likely to be different across preparations, and potentially across temperatures. There are many different processes that drive gastric mill rhythms including release of hormonal peptides such as crustacean cardioactive peptide (CCAP) (Weimann et al., 1997), FLRFamides (Heinzel et al., 1993; Weimann et al., 1993; Christie et al., 2004), pyrokinins (Saideman et al., 2007b; Dickinson et al., 2015), and Gly^1-SIFamide (Blitz et al., 2019). Synaptically released peptides *C. borealis* tachykinin related peptide (CabTRP Ia) (Blitz et al., 1999; Wood et al., 2000) and *C. borealis* pyrokinin peptide I & II (CabPK) (Saideman et al., 2007a; Saideman et al., 2007b) generate similar gastric mill rhythms, while proctolin (Blitz et al., 1999; Stein et al., 2007) excites all gastric mill motor neurons.

Stimulation of certain projection neuron such as MCN1 (contains CabTRP, proctolin, and GABA) (Coleman and Nusbaum, 1994; Coleman et al., 1995; Bartos and Nusbaum, 1997), MCN5 (contains Gly^1-SIFamide) (Norris et al., 1996; Blitz et al., 2019), MCN7 (contains proctolin) (Blitz et al., 1999), CPN2 (Norris et al., 1994), and IVN (the inferior ventricular neurons) (contain FLRFamide and histamine) (Christie et al., 2004), or stimulation of sensory pathways that activate groups of projection neurons (Katz and Harris-Warrick, 1991; Beenhakker et al., 2004; Beenhakker and Nusbaum, 2004; Blitz et al., 2004; Beenhakker et al., 2007; White and Nusbaum, 2011) generate gastric mill rhythms. Because there are so many ways gastric mill rhythms can be generated, and because each method of gastric mill rhythm generation could result in a gastric mill rhythm via a different set of mechanisms, they could have different temperature dependencies. Consequently, we chose to elicit gastric mill rhythms using a single, known mechanism, and we used exogenous stimulation that would reliably produce gastric mill rhythms, that were qualitatively similar to the spontaneous gastric mill rhythms we had previously observed.

A previous study showed that one gastric mill rhythm variant is easily disrupted by small temperature changes (Städele et al., 2015), while the one studied here maintains rhythmicity following a large increase in temperature. Although the functional significance of the diversity among gastric mill rhythms is unclear, the possibility remains that the assortment of gastric mill rhythm generator mechanisms bequeaths a robustness against environmental perturbation. Because there are other versions of the gastric mill not considered here, it will be interesting in the future to

determine the extent to which they are temperature robust and whether, in turn, they are coupled to the pyloric rhythm across temperature.

Temperature compensation is driven by multiple mechanisms

Previous work has shown that neuromodulatory substances can extend the temperature range over which the gastric and pyloric rhythms maintain function (Städele et al., 2015; Haddad and Marder, 2018). In *C. elegans* neuromodulation enhances the robustness of thermosensory neurons and altering temperature dependent behavior (Beverly et al., 2011). Therefore, it is possible that some modulators that act on the STG, not studied here, may further stabilize these rhythms, and some of the modulatory inputs to the STG may release transmitter in response to temperature stress for precisely this reason.

The gastric mill oscillator is activated by both chemical and electrical synapses. In crayfish, the rectifying electrical junction from the lateral giant fiber to the motor giant fiber has reliable synaptic propagation between 20°C and 30°C (Heitler and Edwards, 1998). In a model of this crayfish circuit, Heitler and Edwards (1998) found that if the electrical synapse had a Q_{10} of 11, when most other measured properties of the circuit had Q_{10}s between 2 and 5, the model reliably reproduced physiological responses to temperature increase. In this system, at high temperatures, this increased drive from the electrical synapse offsets the decrease in input resistance of the postsynaptic neuron. In the evoked gastric mill rhythms, CPN2 drives LG and GM via electrical synapses (**Figure 1c**), and our spontaneous rhythms, indicative of CPN2 activation, were observed up to 30°C. While we do not know the Q_{10} of electrical synapses in the STG,

several measured chemical synapses in the pyloric circuit have a Q_{10} of ~2.5 (Tang et al., 2010).

Previous work showed that input resistance modestly decreases in both the Lateral Pyloric (LP) and LG neurons with increased temperature (Tang et al., 2010; Städele et al., 2015). The MCN1–LG electrical synapse may help offset the change in input resistance in the gastric circuit. In the pyloric circuit, the IPSP amplitude in the LP neuron is temperature invariant (Q_{10} ~1), but the IPSC amplitude increased (Q_{10} ~2.5) across the same range of temperatures as those studied here (Tang et al., 2010). The increase in synaptic current may partially compensate for the increase in leak as temperature increases. This could aid circuits in maintaining rhythmicity across temperature. Furthermore, many STG neurons, including both LP and LG, exhibit post-inhibitory rebound (PIR). Both I_A and I_h (currents that promote bursting and PIR) exhibit temperature dependent increases in activation rate and peak current (Q_{10}s ~2 – 4) (Tang et al., 2010).

Circuits are robust to global perturbation

Although it may not be uniformly true that all neuronal circuits maintain coordinated function across a wide range of temperatures in cold blooded animals, here we demonstrate that for two coupled circuits, where coupling is necessary for proper function, coordination is maintained despite a global perturbation. Because each circuit's oscillations arise from a different set of circuit and cellular mechanisms, it is unlikely that the underlying processes endowing temperature compensation are the

same. Therefore, it was not necessarily expected that compensation would be similar for both circuits.

The nervous systems of small homeotherms such as birds, rodents (Chaffee and Roberts, 1971; Janssen, 1992), and even human infants (Mank et al., 2016; Barbi et al., 2017) likely face similar challenges as a result of fluctuations in ambient temperature or in fever response to illness. Although they have homeostatic processes that regulate internal temperature shifts, these regulatory responses can be slow compared to temperature change (Cheshire, 2016). Therefore, it is likely that their nervous systems must be robust to some degree of temperature fluctuation to maintain function until a homeostatic process can intervene to restore internal temperature. While mouse brain neuron temperature sensitivities exist in a much narrower range than the crustaceans studied here (Hori et al., 1999), the temperature range we use is well within the range experienced by the crabs naturally.

In this study, we use temperature as a global perturbation. It is possible that coupled neural circuits are similarly robust to other global perturbations, so that coupling is maintained despite transient or chronic changes in ambient conditions. For example, the pyloric oscillator is known to be robust to large changes in pH (Haley et al., 2018) and to fluctuations in extracellular potassium (He et al., 2020). Collectively, these data indicate that the crustacean STG (and likely many other neural circuits) are capable of sustaining normal output when challenged with global perturbations. While the processes that confer robustness may be different for different circuits and perturbations, nervous systems have likely evolved to cope with a variety of environmental changes.

Methods

Animals and dissection

Adult male Jonah crabs (*C. borealis*; *N* = 19 were obtained from Commercial Lobster (Boston, MA) and *N* = 9 from Moody's Seafood (Brunswick, ME)) and kept in tanks with circulating artificial sea water at 11°C for approximately one week prior to use. Preparations with spontaneous rhythms (*N* = 9), were from crabs caught in July of 2013 and studied soon thereafter. Preparations in which rhythms were evoked (*N* = 10) were from crabs caught July, Sept., and Dec. of 2017. Preparations in which the pyloric pacemaker was inhibited (*N* = 9), were from crabs caught Aug. and Sept. 2020. Thirty minutes prior to dissection, animals were chilled on ice. Dissections were carried out as previously described (Gutierrez and Grashow, 2009) and the dissected nervous systems were kept in chilled saline solution (440 mM NaCl, 11 mM KCl, 26 mM $MgCl_2$, 13 mM $CaCl_2$, 11 mM Trizma base, 5 mM maleic acid, pH 7.45 at 23°C) throughout the dissection. Each dissected stomatogastric nervous system was pinned out in a petri dish with a Sylgard-lined bottom and fresh saline was continuously superfused across the nervous system for the duration of the experiment (**Fig. 1a**).

Nerve Recordings

Motor neuron action potentials originating in the STG (**Fig. 1a**) were recorded extracellularly (**Fig. 1b**) from the nerves via stainless steel pin electrodes. Stretches of the *lgn*, *dgn*, *mvn*, *lvn*, and *pdn* were electrically isolated from the bath with Vaseline wells. Voltage signals were amplified using model 3500 amplifiers (A-M Systems) and digitized at 10 kHz using a Digidata 1440 A-D converter (Axon Instruments/ Molecular

Devices). Data were recorded using pClamp data acquisition software (Axon Instruments/Molecular Devices, version 10.5).

Temperature Control

Saline temperature was monitored continuously using a temperature controller (model CL-100, Warner Instruments) and altered during each experiment using an associated Peltier device and thermocouple (SC-20 and TA-29, Warner Instruments). Saline inflow to the nervous system was positioned within 1 cm of the STG so that the measured temperature at the point of inflow was approximately that of the ganglion somata.

Gastric Mill Rhythm Stimulation

We bilaterally stimulated the dorsal posterior esophageal nerves (*dpons*) to elicit a gastric mill rhythm (**Figure 1a & b**). Stainless steel pin electrodes were placed on either side of each *dpon* and were sealed to the nerve using Vaseline. Stimuli were delivered using a model 3800 stimulator (A-M Systems) via model 3820 stimulus isolation units (A-M Systems). Ten, six-second long episodic stimulus trains (0.6 Hz) were used to evoke gastric mill rhythms using a within-train stimulus rate of 15 Hz, as described in Beenhakker and Nusbaum (2004). The *dpons* contain axons of the ventral cardiac neurons (VCNs) that activate the MCN1 and CPN2, resulting in a VCN-gastric mill rhythm that is often active for tens of minutes (Beenhakker et al., 2004; Beenhakker and Nusbaum, 2004; Blitz and Nusbaum, 2008). The duration of each stretch of gastric mill activity is not consistent either within an experiment at different temperatures or across experiments at the same temperature. Thus, the time between each gastric mill rhythm stimulation was different both between temperatures and across preparations.

Defining gastric mill rhythm variants

While evoked gastric mill rhythms are distinguished by the method used to drive them, in the case of spontaneous gastric mill rhythms, the phase relationships and timing of the gastric mill neurons are used to classify them (White and Nusbaum, 2011).

Recordings from the *mvn* show the Inferior Cardiac (IC) neuron and ventricular dilator (VD) neuron (**Fig. 1b**). Although in the absence of a gastric mill rhythm, the IC and VD neurons are typically active in time with the LP neuron and the Pyloric neurons (PY_5; there are approximately five PY neurons in each preparation) respectively, the initiation of a gastric mill rhythm will often shift the IC and VD neurons into gastric mill timing as shown in **Figure 1b**. Because the timing of the IC and VD neurons are state-dependent, they can aid in classifying spontaneous gastric mill rhythms.

In this study, spontaneous gastric mill rhythms resemble VCN-rhythms as IC and VD activity is restricted to the LG interburst interval, which is known to occur because of CPN2 and LG inhibition of the IC and VD neurons respectively. Additionally, the LG bursts in these spontaneous rhythms did not exhibit any obvious interruptions, as is the case for another gastric mill rhythm that is similar to a VCN-rhythm, save for this difference (White and Nusbaum, 2011).

Spontaneous and evoked gastric mill rhythm temperature ranges

In one set of experiments ($N = 9$), spontaneous gastric mill rhythms were observed. Here, temperature was increased from 11°C to 33°C in 2°C increments, and a given temperature step was held for at least 2 minutes. Time between steps was ~2 minutes.

For experiments in which gastric mill rhythms were evoked ($N = 10$), the temperature was increased in either 2°C or 4°C steps starting at 7°C until a gastric mill rhythm could no longer be evoked (typically 21°C or 23°C). Each temperature step was held for the duration of evoked gastric mill activity, and only after the epoch of the gastric mill rhythm terminated was the temperature advanced to the next step. The time between temperature steps was ~2 minutes.

The VCN-gastric mill rhythms were difficult to generate consistently above 23°C, and in some cases only persisted for several cycles. In some preparations, 19°C was the warmest temperature that a gastric mill rhythm could be evoked. Because the stimulation paradigm only activates a subset of projection neurons in the CoGs, these manipulations may fail to characterize the full extent to which the gastric mill circuit can maintain rhythmicity across temperature. Within the temperature range in which they were readily evoked, gastric mill rhythms lasted for tens of minutes.

Evoked rhythms with AB/PD hyperpolarized

To study the effect of temperature on VCN-gastric mill rhythm alone, in a separate set of experiments, gastric mill rhythms were evoked twice at 11°C, 15°C, 19°C, and 21°C with the pyloric pacemaker both active and inactive at each temperature step ($N = 9$). To inactivate the pyloric pacemaker, each PD neuron was impaled with a single bridge balanced sharp electrode in a current clamp configuration. PD neurons were identified by briefly hyperpolarizing the membrane potential and monitoring the number of spikes recorded extracellularly on the *pdn*. Action potentials from both PD neurons can be monitored on a single *pdn*. Because the electrical coupling between the AB and PD neurons is strong (Maynard and Selverston, 1975; Shruti et al., 2014), it is not necessary

to hyperpolarize all three neurons. PD neurons were targeted because of their relatively large size compared to the AB neuron. Because neurons swell with increased temperature (Tang et al., 2010), it can be difficult to maintain intracellular recordings, especially of small neurons, and not damage the cells.

Data analysis

Spike identification and sorting

To reliably identify spikes from extracellular traces, we wrote spike sorting software that uses supervised machine learning to learn the shape of spikes from a small manually labelled dataset. This software is freely available at https://github.com/sg-s/crabsort. PD, LG and DG neuron spikes were identified on the *pdn*, *lgn* and *dgn* nerves recorded extracellularly. In a small subset of the full data, spikes from these neurons were identified using thresholding, dimensionality reduction of the full spike shape, and manual labelling. Using this subset, we trained a fully connected neural network to classify putative identified spikes in new data. The accuracy of the classification was constantly monitored during sorting, and new annotations were used to continuously re-train the network using an active learning framework. Classification accuracy always exceeded 98%.

After the neural network classified putative spikes in a new dataset, to ensure high-quality spike annotation: 1) we manually inspected the data in two-minute chunks to ensure that no artifacts were accidentally labelled as spikes; 2) we used tools built-in to the spike sorting software to visually inspect, at high-temporal resolution, spikes that

the neural network reported with low confidence; and 3) we used other built-in tools to inspect spikes that differed statistically from other spikes in its class. These steps let us generate high-quality spike annotations for PD, LG, and DG, even when these neurons were partially obscured by other units or noise.

Detection of bursts and measurement of burst metrics

Bursts in PD, LG or DG were defined using inter-spike intervals (ISIs). ISIs longer than 1 second on LG or DG were defined to be an inter-burst interval and were used to annotate the start of a burst. Spikes were considered to be part of a burst only if there were at least n spikes per burst, with $n = 5$ for LG and DG and $n = 2$ for PD.

This method allowed us to identify all burst starts, burst stops, and therefore burst durations and burst periods for every burst. We computed the duty cycle on a cycle-by-cycle basis by dividing the burst duration by the burst period.

Estimation and comparison of Q_{10}s (Figure 4)

The Q_{10} of a process is defined as the factor by which it changes over a ten-degree increment in temperature. We computed the Q_{10} of PD and LG burst periods at every temperature using

$$Q_{10} = \langle \left(\frac{f_T}{f_{11}}\right)^{\frac{10}{T-11}} \rangle$$

where f_T is the mean burst frequency at temperature T and f_{11} is the mean burst frequency at 11°C (the reference temperature).

To compare the Q_{10}s of the pyloric and gastric rhythms, we used a paired t-test and compared the mean Q_{10}s averaged across each preparation. Each animal thus contributed equally and we included all 10 preparations. t represents the test statistic.

Integer coupling analysis (Fig. 5)

To measure the integer coupling between PD burst periods and LG or DG burst periods (**Fig. 5b, c**), we computed the mean burst period of all PD bursts within one LG/DG burst period. Thus, every dot corresponds to one LG burst and all the PD bursts that occur within that LG burst period. LG/DG burst periods are plotted on the vertical axis and the mean PD burst period is plotted on the horizontal axis.

To determine if these burst periods are significantly integer coupled (**Fig. 5d**), we computed the significand (defined here as the value after the decimal point) of the ratio of the ordinate to the abscissa for each dot in **Fig. 5b,c**. For example, if an LG burst had a period of 10.1 seconds, and the mean PD period during that LG burst was 1 second, the significand would be 0.1. If the LG burst period was 9.9 seconds, the significand would be 0.9. We sorted all significands for LG and DG and bootstrapped the data 1000 times to estimate confidence intervals of cumulative density functions of the significands. Shading in **Figure 5d** indicates these confidence intervals. Curves that deviated substantially from the diagonal (the null distribution) corresponded to significant integer coupling between the gastric mill and pyloric burst periods. To determine if any set of significands was significantly different from the null distribution, we performed a

two-sample Kolmogorov-Smirnoff test comparing the significands from the ratios of LG/DG to PD burst periods and significands from ratios of shuffled copies of LG/DG and PD burst periods. The reason we used a two-sample Kolmogorov-Smirnoff test, and not a one-sample test that compares to a uniform distribution directly, is that we cannot expect significands to be distributed exactly uniformly, even for randomly distributed data. We observed through numerical calculations that for certain combinations of numerator (gastric cycle period) and denominator (pyloric cycle period) ranges, even randomly sampled cycle periods can lead to non-uniform significand distributions. The threshold for significance was divided by the number of comparisons (9 temperature steps) to correct for multiple comparisons. Data in **Fig. 5d** are pooled across all preparations and across all temperatures. Statistical tests were performed grouping by temperature, but pooling across all preparations. *D* indicates the Kolmogorov-Smirnoff test statistic.

The dotted and dashed lines in **Fig. 5d** indicate two extremes of the significand distribution. If the gastric and pyloric burst periods were perfectly integer coupled, then every significand of every ratio of periods would be 0 (or 1). Thus, the cumulative probability of such an idealized distribution would be a step-like function shown by the dotted line. On the other extreme, if the ratios of gastric to pyloric burst periods were such that the significands were randomly and uniformly distributed across the unit line (suggesting no integer coupling whatsoever), then the cumulative probability of such a distribution would be close to a diagonal line with unit slope, shown by the dashed line.

These two extremes allow us to define a yardstick to measure the degree of integer coupling for any observed spike train. We observe that all possible cumulative

distributions are bounded by the two extremal distributions (dotted line and dashed line). Because the area of the square in **Fig. 5d** is 1, simple geometry tells us that the area bounded by the maximal distributions is 0.25. We therefore quantified the degree of integer coupling of the two burst periods (**Fig. 5e**) by measuring the area between the null distribution (dashed diagonal line) and the significand c.d.f.

Generation of burst-aligned rasters of PD (Fig. 6a,d)

To visualize the interaction between pyloric and gastric mill rhythms, we generated burst-aligned rasters of the PD neuron activity in which we aligned PD rasters to the burst start in a gastric mill-timed neuron (LG or DG). For every burst start in LG/DG, we plotted the raster of PD spikes centered around that burst start, showing spikes 3 seconds before the burst start in LG/DG and 3 seconds after.

Estimation of gastric mill spike and burst start probability in PD phase (Fig. 6)

To estimate when the LG or DG neurons start bursting in the PD cycle (**Fig. 6**), we first identified the burst start times of LG and DG. At these points, we estimated the PD phase by dividing the time since the start of the previous PD burst by the burst period of that PD cycle. This method of phase estimation assumes that the phase increases uniformly and linearly over a PD cycle, following earlier work (Prinz et al., 2004; Bucher et al., 2005). We used a similar procedure to estimate gastric mill spike probability in PD phase.

Analysis of distribution of LG/DG burst starts in PD phase (Fig. 6 b,e)

LG burst starts in PD time follow circular statistics, since a LG burst start occurring at a PD phase of 1 is the same as a LG burst start at a PD phase of 0. We therefore used a circular statistics toolbox by Phillipp Berens (Berens, 2009) (http://www.eye-tuebingen.de/berenslab/technology-development/) to analyze this data. Means and standard deviations of LG and DG burst starts (**Fig. 6b** inset and **Fig. 6e** inset) were computed using this circular statistics toolbox. To test if LG and DG burst starts were significantly non-uniformly distributed, we used the Rayleigh test for non-uniformity. *z* is the Rayleigh test statistic. The distribution of burst starts of LG or DG in PD time for each preparation, at each temperature was tested for non-uniformity individually.

The number of LG/DG burst starts was not the same for every preparation at every temperature step. For this reason, and to avoid time-dependent confounds, we analyzed the first 40 burst starts for each preparation at each temperature step. Preparation and temperature combinations where there were fewer than 40 burst starts (~35% of data) were excluded. A total of n= 3816 LG burst starts and n=3228 DG burst starts across 9 temperature points and 10 preparations are plotted in **Fig. 6b, d**.

References

Bahramisharif A, Mazaheri A, Levar N, Richard Schuurman P, Figee M, Denys D (2016) Deep Brain Stimulation Diminishes Cross-Frequency Coupling in Obsessive-Compulsive Disorder. Biol Psychiatry 80:e57-58.

Barbi E, Marzuillo P, Neri E, Naviglio S, Krauss BS (2017) Fever in Children: Pearls and Pitfalls. Children (Basel) 4:81.

Bartos M, Nusbaum MP (1997) Intercircuit control of motor pattern modulation by presynaptic inhibition. J Neurosci 17:2247-2256.

Bartos M, Manor Y, Nadim F, Marder E, Nusbaum MP (1999) Coordination of fast and slow rhythmic neuronal circuits. J Neurosci 19:6650-6660.

Beenhakker MP, Nusbaum MP (2004) Mechanosensory activation of a motor circuit by coactivation of two projection neurons. J Neurosci 24:6741-6750.

Beenhakker MP, Blitz DM, Nusbaum MP (2004) Long-lasting activation of rhythmic neuronal activity by a novel mechanosensory system in the crustacean stomatogastric nervous system. J Neurophysiol 91:78-91.

Beenhakker MP, Kirby MS, Nusbaum MP (2007) Mechanosensory gating of proprioceptor input to modulatory projection neurons. J Neurosci 27:14308-14316.

Berens P (2009) CircStat: A MATLAB Toolbox for Circular Statistics. Journal of Statistical Software; Vol 1, Issue 10 (2009).

Beverly M, Anbil S, Sengupta P (2011) Degeneracy and neuromodulation among thermosensory neurons contribute to robust thermosensory behaviors in *Caenorhabditis elegans*. J Neurosci 31:11718-11727.

Blitz DM (2017) Circuit feedback increases activity level of a circuit input through interactions with intrinsic properties. J Neurophysiol 118:949-963.

Blitz DM, Nusbaum MP (2008) State-dependent presynaptic inhibition regulates central pattern generator feedback to descending inputs. J Neurosci 28:9564-9574.

Blitz DM, Nusbaum MP (2012) Modulation of circuit feedback specifies motor circuit output. J Neurosci 32:9182-9193.

Blitz DM, Beenhakker MP, Nusbaum MP (2004) Different sensory systems share projection neurons but elicit distinct motor patterns. J Neurosci 24:11381-11390.

Blitz DM, Christie AE, Cook AP, Dickinson PS, Nusbaum MP (2019) Similarities and differences in circuit responses to applied Gly(1)-SIFamide and peptidergic (Gly(1)-SIFamide) neuron stimulation. J Neurophysiol 121:950-972.

Blitz DM, Christie AE, Coleman MJ, Norris BJ, Marder E, Nusbaum MP (1999) Different proctolin neurons elicit distinct motor patterns from a multifunctional neuronal network. J Neurosci 19:5449-5463.

Bucher D, Prinz AA, Marder E (2005) Animal-to-Animal Variability in Motor Pattern Production in Adults and during Growth. The Journal of Neuroscience 25:1611-1619.

Burrows M (1989) Effects of temperature on a central synapse between identified motor neurons in the locust. Journal of Comparative Physiology A 165:687-695.

Cao XJ, Oertel D (2005) Temperature affects voltage-sensitive conductances differentially in octopus cells of the mammalian cochlear nucleus. J Neurophysiol 94:821-832.

Caplan JS, Williams AH, Marder E (2014) Many parameter sets in a multicompartment model oscillator are robust to temperature perturbations. J Neurosci 34:4963-4975.

Chaffee RRJ, Roberts JC (1971) Temperature Acclimation in Birds and Mammals. Annual Review of Physiology 33:155-202.

Cheshire WP (2016) Thermoregulatory disorders and illness related to heat and cold stress. Autonomic Neuroscience 196:91-104.

Christie AE, Stein W, Quinlan JE, Beenhakker MP, Marder E, Nusbaum MP (2004) Actions of a histaminergic/peptidergic projection neuron on rhythmic motor patterns in the stomatogastric nervous system of the crab *Cancer borealis*. J Comp Neurol 469:153-169.

Coleman MJ, Nusbaum MP (1994) Functional consequences of compartmentalization of synaptic input. J Neurosci 14:6544-6552.

Coleman MJ, Meyrand P, Nusbaum MP (1995) A switch between two modes of synaptic transmission mediated by presynaptic inhibition. Nature 378:502-505.

Colgin LL (2011) Oscillations and hippocampal–prefrontal synchrony. Current Opinion in Neurobiology 21:467-474.

de Hemptinne C, Ryapolova-Webb ES, Air EL, Garcia PA, Miller KJ, Ojemann JG, Ostrem JL, Galifianakis NB, Starr PA (2013) Exaggerated phase-amplitude coupling in the primary motor cortex in Parkinson disease. Proc Natl Acad Sci U S A 110:4780-4785.

DeLong ND, Kirby MS, Blitz DM, Nusbaum MP (2009) Parallel regulation of a modulator-activated current via distinct dynamics underlies comodulation of motor circuit output. J Neurosci 29:12355-12367.

Dickinson PS, Kurland SC, Qu X, Parker BO, Sreekrishnan A, Kwiatkowski MA, Williams AH, Ysasi AB, Christie AE (2015) Distinct or shared actions of peptide family isoforms: II. Multiple pyrokinins exert similar effects in the lobster stomatogastric nervous system. J Exp Biol 218:2905-2917.

Diehl F, White RS, Stein W, Nusbaum MP (2013) Motor circuit-specific burst patterns drive different muscle and behavior patterns. J Neurosci 33:12013-12029.

Du Y, Lu Q, Wang R (2010) Using interspike intervals to quantify noise effects on spike trains in temperature encoding neurons. Cognitive Neurodynamics 4:199-206.

Fohlmeister JF, Cohen ED, Newman EA (2010) Mechanisms and distribution of ion channels in retinal ganglion cells: using temperature as an independent variable. J Neurophysiol 103:1357-1374.

Fonseca PJ, Correia T (2007) Effects of temperature on tuning of the auditory pathway in the cicada Tettigetta josei (*Hemiptera, Tibicinidae*). J Exp Biol 210:1834-1845.

Foster JA, Robertson RM (1992) Temperature Dependency of Wing-Beat Frequency in Intact and Deafferented Locusts. Journal of Experimental Biology 162:295-312.

Franz A, Ronacher B (2002) Temperature dependence of temporal resolution in an insect nervous system. Journal of Comparative Physiology A 188:261-271.

Fujisawa S, Buzsáki G (2011) A 4 Hz oscillation adaptively synchronizes prefrontal, VTA, and hippocampal activities. Neuron 72:153-165.

Garrity PA, Goodman MB, Samuel AD, Sengupta P (2010) Running hot and cold: behavioral strategies, neural circuits, and the molecular machinery for thermotaxis in *C. elegans* and *Drosophila*. Genes & Development 24:2365-2382.

Gordon JA (2011) Oscillations and hippocampal-prefrontal synchrony. Current opinion in neurobiology 21:486-491.

Gutierrez GJ, Grashow RG (2009) *Cancer borealis* stomatogastric nervous system dissection. J Vis Exp:https://www.ncbi.nlm.nih.gov/pubmed/19308017.

Gutierrez GJ, O'Leary T, Marder E (2013) Multiple mechanisms switch an electrically coupled, synaptically inhibited neuron between competing rhythmic oscillators. Neuron 77:845-858.

Haddad SA, Marder E (2018) Circuit Robustness to Temperature Perturbation Is Altered by Neuromodulators. Neuron 100:609-623 e603.

Haley JA, Hampton D, Marder E (2018) Two central pattern generators from the crab, Cancer borealis, respond robustly and differentially to extreme extracellular pH. Elife 7.

Hamood AW, Marder E (2015) Consequences of acute and long-term removal of neuromodulatory input on the episodic gastric rhythm of the crab Cancer borealis. J Neurophysiol 114:1677-1692.

Harris AZ, Gordon JA (2015) Long-range neural synchrony in behavior. Annu Rev Neurosci 38:171-194.

Hazel JR, Prosser CL (1974) Molecular mechanisms of temperature compensation in poikilotherms. Physiol Rev 54:620-677.

He LS, Rue MCP, Morozova EO, Powell DJ, James EJ, Kar M, Marder E (2020) Rapid adaptation to elevated extracellular potassium in the pyloric circuit of the crab, *Cancer borealis*. Journal of Neurophysiology 123:2075-2089.

Heinzel HG, Weimann JM, Marder E (1993) The behavioral repertoire of the gastric mill in the crab, *Cancer pagurus*: an *in situ* endoscopic and electrophysiological examination. J Neurosci 13:1793-1803.

Heitler WJ, Edwards DH (1998) Effect of temperature on a voltage-sensitive electrical synapse in crayfish. The Journal of Experimental Biology 201:503.

Hori A, Minato K, Kobayashi S (1999) Warming-activated channels of warm-sensitive neurons in rat hypothalamic slices. Neuroscience Letters 275:93-96.

Jacobson TK, Howe MD, Schmidt B, Hinman JR, Escabi MA, Markus EJ (2013) Hippocampal theta, gamma, and theta-gamma coupling: effects of aging, environmental change, and cholinergic activation. J Neurophysiol 109:1852-1865.

Janssen R (1992) Thermal influences on nervous system function. Neuroscience & Biobehavioral Reviews 16:399-413.

Kang K, Panzano VC, Chang EC, Ni L, Dainis AM, Jenkins AM, Regna K, Muskavitch MAT, Garrity PA (2012) Modulation of TRPA1 thermal sensitivity enables sensory discrimination in *Drosophila*. Nature 481:76-80.

Karalis N, Dejean C, Chaudun F, Khoder S, Rozeske RR, Wurtz H, Bagur S, Benchenane K, Sirota A, Courtin J, Herry C (2016) 4-Hz oscillations synchronize prefrontal–amygdala circuits during fear behavior. Nature Neuroscience 19:605-612.

Katz PS, Harris-Warrick RM (1991) Recruitment of crab gastric mill neurons into the pyloric motor pattern by mechanosensory afferent stimulation. J Neurophysiol 65:1442-1451.

Kirihara K, Rissling AJ, Swerdlow NR, Braff DL, Light GA (2012) Hierarchical organization of gamma and theta oscillatory dynamics in schizophrenia. Biol Psychiatry 71:873-880.

Klockner U, Schiefer A, Isenberg G (1990) L-type Ca-channels: similar Q10 of Ca-, Ba- and Na-conductance points to the importance of ion-channel interaction. Pflugers Arch 415:638-641.

Kushinsky D, Morozova EO, Marder E (2019) In vivo effects of temperature on the heart and pyloric rhythms in the crab *Cancer borealis*. J Exp Biol 222.

Lisman J (2005) The theta/gamma discrete phase code occuring during the hippocampal phase precession may be a more general brain coding scheme. Hippocampus 15:913-922.

Lisman J, Buzsáki G (2008) A Neural Coding Scheme Formed by the Combined Function of Gamma and Theta Oscillations. Schizophrenia Bulletin 34:974-980.

Lisman JE, Jensen O (2013) The θ-γ neural code. Neuron 77:1002-1016.

Long MA, Fee MS (2008) Using temperature to analyse temporal dynamics in the songbird motor pathway. Nature 456:189-194.

Mank A, van Zanten HA, Meyer MP, Pauws S, Lopriore E, Te Pas AB (2016) Hypothermia in Preterm Infants in the First Hours after Birth: Occurrence, Course and Risk Factors. PLoS One 11:e0164817-e0164817.

Marder E, Bucher D (2007) Understanding circuit dynamics using the stomatogastric nervous system of lobsters and crabs. Annu Rev Physiol 69:291-316.

Marder E, Manor Y, Nadim F, Bartos M, Nusbaum MP (1998) Frequency control of a slow oscillatory network by a fast rhythmic input: pyloric to gastric mill interactions in the crab stomatogastric nervous system. Ann N Y Acad Sci 860:226-238.

Marder E, Haddad SA, Goeritz ML, Rosenbaum P, Kispersky T (2015) How can motor systems retain performance over a wide temperature range? Lessons from the crustacean stomatogastric nervous system. J Comp Physiol A Neuroethol Sens Neural Behav Physiol 201:851-856.

Maynard DM, Selverston AI (1975) Organization of the stomatogastric ganglion of the spiny lobster. Journal of comparative physiology 100:161-182.

Meyrand P, Simmers J, Moulins M (1994) Dynamic construction of a neural network from multiple pattern generators in the lobster stomatogastric nervous system. J Neurosci 14:630-644.

Montgomery SM, Buzsaki G (2007) Gamma oscillations dynamically couple hippocampal CA3 and CA1 regions during memory task performance. Proc Natl Acad Sci U S A 104:14495-14500.

Moran LV, Hong LE (2011) High vs low frequency neural oscillations in schizophrenia. Schizophr Bull 37:659-663.

Moran MM, Xu H, Clapham DE (2004) TRP ion channels in the nervous system. Curr Opin Neurobiol 14:362-369.

Nadim F, Manor Y, Nusbaum MP, Marder E (1998) Frequency regulation of a slow rhythm by a fast periodic input. J Neurosci 18:5053-5067.

Norris BJ, Coleman MJ, Nusbaum MP (1994) Recruitment of a projection neuron determines gastric mill motor pattern selection in the stomatogastric nervous system of the crab, *Cancer borealis*. J Neurophysiol 72:1451-1463.

Norris BJ, Coleman MJ, Nusbaum MP (1996) Pyloric motor pattern modification by a newly identified projection neuron in the crab stomatogastric nervous system. J Neurophysiol 75:97-108.

O'Leary T, Marder E (2016) Temperature-Robust Neural Function from Activity-Dependent Ion Channel Regulation. Curr Biol 26:2935-2941.

Prinz AA, Bucher D, Marder E (2004) Similar network activity from disparate circuit parameters. Nat Neurosci 7:1345-1352.

Prosser CL, Nelson DO (1981) The Role of Nervous Systems in Temperature Adaptation of Poikilotherms. Annual Review of Physiology 43:281-300.

Ramot D, MacInnis BL, Goodman MB (2008) Bidirectional temperature-sensing by a single thermosensory neuron in *C. elegans*. Nature Neuroscience 11:908-915.

Rinberg A, Taylor AL, Marder E (2013) The effects of temperature on the stability of a neuronal oscillator. PLoS Comput Biol 9:e1002857.

Robertson RM, Money TGA (2012) Temperature and neuronal circuit function: compensation, tuning and tolerance. Current Opinion in Neurobiology 22:724-734.

Roemschied FA, Eberhard MJB, Schleimer J-H, Ronacher B, Schreiber S (2014) Cell-intrinsic mechanisms of temperature compensation in a grasshopper sensory receptor neuron. eLife 3:e02078.

Rojas-Líbano D, Frederick DE, Egaña JI, Kay LM (2014) The olfactory bulb theta rhythm follows all frequencies of diaphragmatic respiration in the freely behaving rat. Front Behav Neurosci 8:214-214.

Saideman SR, Blitz DM, Nusbaum MP (2007a) Convergent motor patterns from divergent circuits. J Neurosci 27:6664-6674.

Saideman SR, Ma M, Kutz-Naber KK, Cook A, Torfs P, Schoofs L, Li L, Nusbaum MP (2007b) Modulation of rhythmic motor activity by pyrokinin peptides. J Neurophysiol 97:579-595.

Salimpour Y, Anderson WS (2019) Cross-Frequency Coupling Based Neuromodulation for Treating Neurological Disorders. Frontiers in Neuroscience 13.

Scheffer-Teixeira R, Tort ABL (2016) On cross-frequency phase-phase coupling between theta and gamma oscillations in the hippocampus. eLife 5:e20515.

Schleimer J-H, Schreiber S (2016) Homeostasis: How Neurons Achieve Temperature Invariance. Current Biology 26:R1141-R1143.

Shruti S, Schulz DJ, Lett KM, Marder E (2014) Electrical coupling and innexin expression in the stomatogastric ganglion of the crab *Cancer borealis*. Journal of Neurophysiology 112:2946-2958.

Soofi W, Goeritz ML, Kispersky TJ, Prinz AA, Marder E, Stein W (2014) Phase maintenance in a rhythmic motor pattern during temperature changes *in vivo*. J Neurophysiol 111:2603-2613.

Städele C, Heigele S, Stein W (2015) Neuromodulation to the Rescue: Compensation of Temperature-Induced Breakdown of Rhythmic Motor Patterns via Extrinsic Neuromodulatory Input. PLoS Biol 13:e1002265.

Stehlik LL, MacKenzie Jr. CL, Morse WW (1991) Distribution and abundance of four brachyuran crabs on the northwest atlantic shelf. Fishery Bulletin, US:473-492.

Stein W, DeLong ND, Wood DE, Nusbaum MP (2007) Divergent co-transmitter actions underlie motor pattern activation by a modulatory projection neuron. Eur J Neurosci 26:1148-1165.

Stiebler IB, Narins PM (1990) Temperature-dependence of auditory nerve response properties in the frog. Hearing Research 46:63-81.

Tamura M, Spellman TJ, Rosen AM, Gogos JA, Gordon JA (2017) Hippocampal-prefrontal theta-gamma coupling during performance of a spatial working memory task. Nature Communications 8:2182.

Tang LS, Taylor AL, Rinberg A, Marder E (2012) Robustness of a rhythmic circuit to short- and long-term temperature changes. J Neurosci 32:10075-10085.

Tang LS, Goeritz ML, Caplan JS, Taylor AL, Fisek M, Marder E (2010) Precise Temperature Compensation of Phase in a Rhythmic Motor Pattern. PLOS Biology 8:e1000469.

Tass P, Rosenblum MG, Weule J, Kurths J, Pikovsky A, Volkmann J, Schnitzler A, Freund HJ (1998) Detection of *n:m* Phase Locking from Noisy Data: Application to Magnetoencephalography. Physical Review Letters 81:3291-3294.

Weimann JM, Marder E (1994) Switching neurons are integral members of multiple oscillatory networks. Curr Biol 4:896-902.

Weimann JM, Meyrand P, Marder E (1991) Neurons that form multiple pattern generators: identification and multiple activity patterns of gastric/pyloric neurons in the crab stomatogastric system. J Neurophysiol 65:111-122.

Weimann JM, Marder E, Evans B, Calabrese RL (1993) The effects of SDRNFLRFamide and TNRNFLRFamide on the motor patterns of the stomatogastric ganglion of the crab *Cancer borealis*. J Exp Biol 181:1-26.

Weimann JM, Skiebe P, Heinzel HG, Soto C, Kopell N, Jorge-Rivera JC, Marder E (1997) Modulation of oscillator interactions in the crab stomatogastric ganglion by crustacean cardioactive peptide. J Neurosci 17:1748-1760.

White RS, Nusbaum MP (2011) The same core rhythm generator underlies different rhythmic motor patterns. J Neurosci 31:11484-11494.

Wood DE, Stein W, Nusbaum MP (2000) Projection neurons with shared cotransmitters elicit different motor patterns from the same neural circuit. J Neurosci 20:8943-8953.

Xu H, Robertson RM (1994) Effects of temperature on properties of flight neurons in the locust. Journal of Comparative Physiology A 175:193-202.

Xu H, Robertson RM (1996) Neural parameters contributing to temperature compensation in the flight CPG of the locust, *Locusta migratoria*. Brain Research 734:213-222.

Yang F, Zheng J (2014) High temperature sensitivity is intrinsic to voltage-gated potassium channels. eLife 3:e03255.

Zečević D, Levitan H (1980) Temperature acclimation: effects on membrane physiology of an identified snail neuron. American Journal of Physiology-Cell Physiology 239:C47-C57.

Zečević D, Levitan H, Paŝić M (1985) Temperature Acclimation: Influence on Transient Outward and Inward Currents in an Identified Neurone of *Helix pomatia*. Journal of Experimental Biology 117:369.

Zheng C, Bieri KW, Hsiao YT, Colgin LL (2016) Spatial Sequence Coding Differs during Slow and Fast Gamma Rhythms in the Hippocampus. Neuron 89:398-408.